Endogenous microbiota member *Faecalibaculum rodentium* PB1 protects from intestinal tumor growth

Elena Zagato[1]†, Chiara Pozzi[1,2]†, Alice Bertocchi[1], Tiziana Schioppa[3], Fabiana Saccheri[1], Silvia Guglietta[1¶], Bruno Fosso[4], Laura Melocchi[5,6], Giulia Nizzoli[7], Jacopo Troisi[8,9,10], Marinella Marzano[4], Bianca Oresta[1], Ilaria Spadoni[1], Koji Atarashi[11,12], Sara Carloni[13], Stefania Arioli[14], Giulia Fornasa[2], Francesco Asnicar[15], Nicola Segata[16], Simone Guglielmetti[14], Kenya Honda[11,12], Graziano Pesole[4,17], William Vermi[5,18], Giuseppe Penna[2] and Maria Rescigno[1,13,*]

Affiliations:

[1]Department of Experimental Oncology, European Institute of Oncology IRCCS, 20139 Milan, Italy

[2]Humanitas Clinical and Research Center – IRCCS, Via Manzoni 56, 20089 Rozzano – Milan, Italy

[3]Department of Molecular and Translational Medicine, University of Brescia, 25121 Brescia, Italy

[4]Institute of Biomembranes, Bioenergetics and Molecular Biotechnologies (IBIOM), Consiglio Nazionale delle Ricerche, Via Amendola 165/A, 70126 Bari, Italy

[5]Section of Pathology, Department of Molecular and Translational Medicine, University of Brescia, 25121 Brescia, Italy

[6]Pathology Department, Fondazione Poliambulanza Hospital, Brescia

[7]Gastroenterology and Endoscopy Unit, Fondazione IRCCS Cà Granda, Ospedale Maggiore Policlinico, 20122 Milan, Italy

[8]Department of Medicine, Surgery and Dentistry, "Scuola Medica Salernitana", University of Salerno, Via Allende, 84081 Baronissi (SA) Italy

[9]Theoreo srl, spin-off company of the University of Salerno, Via degli Ulivi 3, 84090 Montecorvino Pugliano (SA), Italy

[10]European Biomedical Research Institute of Salerno (EBRIS), Via S. de Renzi, 3, 84125 Salerno, Italy
[11]RIKEN Center for Integrative Medical Sciences (IMS), 1-7-22 Suehiro-cho, Tsurumi-ku, Yokohama, Kanagawa 230-0045, Japan
[12]Department of Microbiology and Immunology, Keio University School of Medicine, 35 Shinanomachi, Shinjuku-ku, Tokyo 160-8582, Japan
[13]Humanitas University Department of Biomedical Sciences, Via Rita Levi Montalcini, 20090 Pieve Emanuele – Milan, Italy
[14]Division of Food Microbiology and Bioprocesses, Department of Food, Environmental and Nutritional Sciences (DeFENS), Università degli Studi di Milano, 20133 Milan, Italy
[15]Department CIBIO, University of Trento, Trento, Italy
[16]Centre for Integrative Biology, University of Trento, 38122 Trento, Italy
[17]Department of Biosciences, Biotechnology and Biopharmaceutics, University of Bari, 70124 Bari, Italy
[18]Department of Pathology and Immunology, Washington University, Saint Louis, MO 63110, USA
[*]Correspondence: maria.rescigno@hunimed.eu
[¶]Present address: Medical University of South Carolina, Department of Microbiology and Immunology, Hollings Cancer Center, 86 Jonathan Lucas St, Charleston, SC (USA)
†These authors contributed equally to this work.

SUMMARY

The microbiota has been shown to promote intestinal tumorigenesis, but a possible anti-tumorigenic effect has also been postulated. Here, we demonstrate that changes in microbiota and mucus composition are concomitant with tumorigenesis. We identified two anti-tumorigenic strains of the microbiota, *Faecalibaculum rodentium* and its human homolog *Holdemanella biformis,* which are strongly underrepresented during tumorigenesis. Reconstitution of $Apc^{Min/+}$ or AOM/DSS-treated mice with an isolate of *F. rodentium* (*F.* PB1) or its metabolic products reduced tumor growth. *F.* PB1 and *H. biformis* produced short-chain fatty acids (SCFAs) that contributed to control protein acetylation and tumor cell proliferation by inhibiting calcineurin/NFATc3 activation both in mouse and human settings. Thus, we have identified endogenous anti-tumorigenic bacterial strains with strong diagnostic, therapeutic and translational potential.

INTRODUCTION

Colorectal cancer (CRC) is the third leading cause of tumor-related deaths. It is a multifactorial disorder influenced by genetic, environmental and lifestyle factors, including the deregulation of the microbiota[1]. A decrease in *Clostridium* and *Bacteroides* and an increase in *Fusobacterium*[2,3] has been reported in CRC, also in association with recurrence[4]. The role of bacteria in tumorigenesis has been extensively demonstrated in spontaneous mouse models of tumorigenesis such as the adenomatous polyposis coli (APC) multiple intestinal neoplasia (Min) ($Apc^{Min/+}$) mice, carrying a mutation in the APC gene which is mutated in more than 80% of sporadic CRC[5]. Microbiota-derived signals drive ERK phosphorylation and increased stability of the oncogene Myc, or trigger the c-Jun/JNK and STAT3 signaling pathways

77 driving cell proliferation and accumulation of suppressive immune cells within the
78 tumor[6] or the exacerbation of the inflammatory response[7]. *Enterotoxigenic*
79 *Bacteroides fragilis* (ETBF)[8] and colibactin-producing *Escherichia coli*[9] exert their
80 protumorigenic effect through bacterial toxins. On the other hand, in an inflammation-
81 induced model of colitis associated CRC, after treatment with azoxymethane (AOM)
82 and dextran sulfate sodium (DSS), germ-free (GF) mice develop significantly more
83 and larger tumors compared with SPF mice[9,10]. Further, GF AOM/DSS treated mice
84 transplanted with fecal microbiota from CRC patients develop more tumors than those
85 transplanted with fecal microbiota from healthy subjects, but again it is not clear
86 whether this is due to an increase in tumor promoting-, a decrease of antitumorigenic-
87 bacteria, or both[11]. Further, a diet rich in fibers can protect against tumor development
88 in a microbiota-dependent manner[12]. Thus, although most studies have concentrated
89 on identifying tumor-promoting bacteria the role and identification of endogenous
90 anti-tumorigenic microbiota remains elusive.
91 Here, we identified an endogenous strain of the mouse microbiota (*Faecalibaculum*
92 *rodentium* PB1, *F.* PB1) and its human counterpart *Holdemanella biformis* belonging
93 to the *Erysipelotrichaceae* family, which are lost during the early phases of
94 tumorigenesis. Reconstitution of mice with *F.* PB1 or *H. biformis* spent medium leads
95 to tumor protection via the release of SCFAs, and in particular butyrate, that act as
96 histone deacetylase inhibitors (HDACi) and block tumor cell proliferation via
97 reducing NFATc3 and calcineurin activation.
98
99 **RESULTS**
100 ***Faecalibaculum rodentium* is underrepresented during the early phases of**
101 **tumorigenesis.**

We followed changes in microbiota composition in a longitudinal study in cohorts of $Apc^{Min/+}$ mice and age- and sex-matched C57BL/6 wild-type (WT) littermates born from the same mothers. Bacterial DNA was extracted at 4, 8 and 12 weeks from feces. As shown in Figures 1a and Extended Data 1a, we did not observe any change in the Shannon, Chao1 and Simpson diversity indexes among the two groups at any age, while we observed differences in genus abundance at 8 and 12 weeks (Figure 1b). Already at 8 weeks, when tumor start developing (Extended Data 1b), and even more so at 12 weeks, we observed a quantitative contraction of the paired end reads (PE) ascribed to the genus *Faecalibaculum* (8 weeks $P<0.01$; 12 weeks $P<0.0005$) in $Apc^{Min/+}$ mice compared to WT littermates. Moreover, we detected an expansion of PE-associated to *Lactobacillus* ($P=0.04$), *Parabacteroides* ($P=0.03$) and *Bacteroides* ($P=0.016$) in $Apc^{Min/+}$ mice compared to WT mice, but only at 12 weeks (Figure 1b). Among the 10 most abundantly represented taxonomic units of WT mice, we found that only the reads ascribed to *Faecalibaculum rodentium*[13] were strongly and significantly underrepresented in $Apc^{Min/+}$ mice compared to WT mice ($P<0.001$). This taxon was not expanded at 8 weeks in $Apc^{Min/+}$ mice, coincident with the initiation of tumor development (Figures 1c and Extended Data 1c). These data were confirmed by qPCR (Figure 1d). To functionally analyze the role of *F. rodentium* in tumor development, we isolated and entirely sequenced a strain belonging to this taxon from WT mice and found that it is the only representative of *F. rodentium* in our mouse WT colony (Figure 1c, not shown). The new isolate named PB1 (hereafter called *F. rodentium* PB1*, F.* PB1), was associated to the mucus of the small and large intestines, but was drastically reduced in mucus from $Apc^{Min/+}$ mice (Figure 1e). Hence, we have identified a strain of *F. rodentium* which is normally highly abundant in WT mice and is strongly under-represented in $Apc^{Min/+}$ mice early in tumorigenesis.

F. PB1 loss coincides with mucus changes and when reintroduced it protects from tumor development

The mucus layer serves as a niche for the intestinal microbiota[14], and changes in its composition are likely to influence the microbiota profile. During tumorigenesis, epithelial cell transformation may result in modification in the production of mucins, the major components of mucus, resulting in a non-permissive environment for *F.* PB1. As shown in Figure 2a, we observed that, similarly to human CRC (hCRC), mucin Muc1 and Muc20[15] were overexpressed, while Muc5ac was aberrantly expressed in tumors, as it is not normally expressed in the lower GI tract[16]. We found a downregulation of Muc3 and Muc13; the latter also in the non-tumoral region of $Apc^{Min/+}$ mice at 8 weeks of age, suggesting that this may be an early event in tumorigenesis. We confirmed at protein level the downregulation of Muc13 both in tumor and non-tumor regions in $Apc^{Min/+}$ mice compared to WT mice, while differently from RNA data, Muc1 and 20 were downregulated in the gut tissue (Extended Data 2a). This may be due to increased secretion into the intestinal lumen as Muc1 was higher in the mucus of $Apc^{Min/+}$ tumors (Extended Data 2b).

Next, we tested whether *F.* PB1 was capable of colonizing $Apc^{Min/+}$ mice. We treated WT or $Apc^{Min/+}$ mice with antibiotics to eliminate competing microorganisms and administered *F.* PB1 by gavage. As shown in Figure 2b, *F.* PB1 was present in ileal mucus of $Apc^{Min/+}$ at 48h, but to a lesser extent than WT mice suggesting that the $Apc^{Min/+}$ gut is unfavorable for *F.* PB1 colonization. This was confirmed by FISH analysis using probes specific for *F.* PB1 (Figure 2c). Thus, to evaluate a possible role of *F.* PB1 in tumor protection, we administered it by gavage every other day to ensure an appreciable level throughout the experiment. We treated $Apc^{Min/+}$ and WT littermates with *F.* PB1 before or during tumor development and evaluated its

capacity to interfere with tumorigenesis. We observed that administration of *F.* PB1 from 4 to 8 weeks did not affect tumor development (Figure 2d). However, administration of *F.* PB1 from week 8 to 12 (i.e. when the bacterium was not enriched in $Apc^{Min/+}$ mice) resulted in a clear reduction in tumor numbers and dimension (Figures 2e,f). The reduction in tumor multiplicity observed macroscopically was no longer statistically significant when we analyzed the number of lesions microscopically (Extended Data 2c), indicating that some small lesions could not be detected by eye and that *F.* PB1 likely affects tumor growth rather than initiation.

Overall, these results suggest that the modification in mucus composition likely creates an unfavorable environment for *F.* PB1 colonization. Administration of *F.* PB1 has an antitumor effect only when tumors have already started developing.

_F._ PB1 affects tumor cell proliferation without major impact on adaptive immune cells

The anti-tumor activity of *F.* PB1 may depend on the immune system. Thus, we assessed the capacity of *F.* PB1 to activate an immune response in the absence of a confounding microbiota, through monocolonization of germ-free (GF) mice. As shown in Extended Data 3, *F.* PB1 did not significantly impact on immune cell development. It did not modify the amount of FoxP3+ T regulatory cells in the small intestine lamina propria and only slightly (but not statistically significant) in the large intestine (Extended Data 3a) and had no effect on IL-17 or IFNγ producing $CD4^+$ T cells at both locations (Extended Data 3b,c). We then analyzed the effect of *F.* PB1 in $Apc^{Min/+}$ mice. We could not detect any difference in the frequencies of all the tested $CD4^+$ T cell populations ($FoxP3^+$ T regulatory cells, Th1 or Th17) in SPF $Apc^{Min/+}$ mice administered with *F.* PB1. However, we observed a trend towards a reduction in

177 their absolute numbers (Figure 3a and Extended Data 3d,e). We then analyzed the
178 innate immune cell components, mononuclear phagocytes and neutrophils. We found
179 no difference in neutrophil frequencies and counts in the small intestinal lamina
180 propria, while we observed a reduction in all of the mononuclear phagocytes in
181 $Apc^{Min/+}$ mice administered with *F.* PB1 (Extended Data 3f,g).
182 Consistent with our previous data[17], we observed a higher frequency, albeit not
183 significant, of circulating $Ly6G^{+}$ $CD11b^{+}$ neutrophils at 12 weeks of age in $Apc^{Min/+}$
184 mice compared to WT littermates[17] regardless of *F.* PB1 treatment. By contrast,
185 treatment with *F.* PB1 resulted in the reduction of circulating $Ly6C^{high}$ $CD11b^{+}$
186 inflammatory monocytes in both WT and $Apc^{Min/+}$ mice (Figure 3b and Extended
187 Data 3h). Hence, the reduction of gut inflammatory monocytes may be due to a
188 reduction of circulating monocytes during *F.* PB1 treatment.
189 We then evaluated whether *F.* PB1 was acting directly on tumor cell growth. We
190 administered *F.* PB1 to 8 weeks old mice and then analyzed tumor growth just two
191 weeks later. *F.* PB1 treatment induced a reduction of: tumor numbers by a
192 macroscopic evaluation (Figure 3c), tumor size (Figure 3d), tumor cell proliferation
193 (Figures 3e and 3f) and rectal bleeding (Figure 3g). Together, these results suggest
194 that *F.* PB1 impacts on tumor cell proliferation.
195 We then analyzed whether *F.* PB1 administration had changed the microbiota
196 composition and its metabolic output. Bacterial DNA was extracted from feces of
197 $Apc^{Min/+}$ mice treated or not with *F.* PB1 and the 16S rRNA gene profiling data were
198 analyzed. We observed an increase in SCFA-producing bacteria in mice treated with
199 *F.* PB1, particularly *Butyricimonas*, butyric acid-producing bacteria[18] (Extended Data
200 4a). As these and the other SCFA-producing bacteria were not reduced in the initial

assessment of microbiota in untreated $Apc^{Min/+}$ versus WT mice during tumor development, it is unlikely that these bacteria impact on tumorigenesis.

It has been reported that $Apc^{Min/+}$ mice deleted for *niacr1* (GPR109A, the receptor for butyrate) are more susceptible to tumor development via a mechanism that depends on the microbiota[19]. Thus, we evaluated whether *F.* PB1 administration may affect the fecal level of SCFAs. We detected an increase in SCFAs (propionate, butyrate and acetate) and a reduction in lactate in the fecal content of *F.* PB1 treated mice at 12 weeks as compared to 8 weeks of age (Figure 3h). No significant differences were observed in succinate and isovalerate while a slight increase in valerate was observed between treated and untreated mice (Extended Data 4b).

These results suggest that *F.* PB1 alone or in cooperation with other bacteria affects tumor cell proliferation, probably via the release of SCFAs.

_F._ PB1 releases SCFAs that have anti-proliferative activity

Butyrate has been described to have histone deacetylase (HDAC) inhibitory activity[20] that affects cell proliferation. This is relevant in CRC cells because, due to the Warburg effect, they undergo increased glycolysis rather than mitochondrial oxidative metabolism[21]. Cancer cells do not use butyrate for their growth as normal epithelial cells and the concentration of butyrate accumulates, acting as HDAC inhibitor while leaving normal cells unaffected[22]. We carried out a dose-dependent response on four different mouse intestinal tumor cell lines (APC, CT26, MC-38 and CMT-93) and found maximal cell growth inhibition, without compromising cell viability at 1-2 mM butyrate, and at a much higher doses of acetate and propionate (2,5-50 mM). We found that the combination of SCFAs additively inhibited the proliferation of all tested cell lines (Figure 4a).

Then we assessed whether *F.* PB1 itself was capable of synthesizing SCFAs *in vitro*. *F.* PB1 grown in strictly anaerobic conditions was very efficient in producing both butyrate and lactate (Figure 4b). Interestingly, the concentration of butyrate (1 mM) was very similar to the one identified on cell lines as capable of inhibiting cell proliferation, while that of acetate or propionate was extremely low (250-5000 times lower than the one effective *in vitro* on cell lines). We then evaluated whether also the *F.* PB1 spent medium (SUP), containing SCFAs, had anti-proliferative activity. As shown in Figure 4c, the addition of SUP drastically inhibited tumor cell proliferation without affecting tumor cell viability (not shown), suggesting that *F.* PB1 releases metabolites that interfere with cell proliferation.

A recent report has shown that tumorigenesis in hCRC and $Apc^{Min/+}$ mice is dependent on a calcineurin-mediated activation of the Nuclear factor of activated T cells (NFAT)c3 transcription factor which is important for cell proliferation[23]. Because the histone deacetylase inhibitor panobinostat can induce calcineurin degradation in multiple myeloma cells[24], we wondered whether the SCFAs produced by *F.* PB1 could act as HDAC inhibitors and therefore affect calcineurin and NFATc3 activation. This would explain why administration of *F.* PB1 or its spent medium could inhibit tumor cell proliferation. Treatment with *F.* PB1 SUP (Figure 4d) or the combination of SCFAs (Extended Data 5a) drastically increased acetylation of histone H3 (H3K27Ac) confirming its HDACi activity. This correlated with the downregulation of calcineurin (PP2B-A) and NFATc3 activation in CRC cell lines (Figure 4d and Extended Data 5b).

SCFAs are volatile and can be extracted through evaporation. Thus, we compared the effect of the untreated *F.* PB1 SUP with one treated by evaporation to deplete SCFAs. As expected, there was a minor effect of SUP evaporation on the concentration of

lactate, still the evaporated SUP was strongly impaired in inducing H3 acetylation and NFATc3 downregulation, suggesting that lactate was not involved in this process (Figures 4e,f and Extended Data 5c). By contrast, there was very little acetate and propionate in the evaporated SUP while the concentration of butyrate was halved. Thus the residual effect on H3 acetylation and NFATc3 downregulation could be due to the left-over of butyrate still present in the supernatant after evaporation (Figure 4f), or to other metabolites not affected by evaporation. Hence, *F.* PB1 releases metabolites, including SCFAs that can impact on tumor cell proliferation by inhibiting HDACs thus blocking NFATc3 and calcineurin activation.

_F._ PB1 metabolic products have anti-proliferative activity _in vivo_ and this is independent on the microbiota

We then evaluated whether the *F.* PB1 SUP had anti-tumorigenic activity *in vivo*. *F.* PB1 SUP did not statistically affect tumor multiplicity, but significantly reduced the size of tumor lesions (Figures 5a,b and Extended Data 6a). We then pretreated 11 weeks old $Apc^{Min/+}$ mice (having already developed tumors) with antibiotics to affect the microbiota but not tumor growth and then the SUP was administered in the presence of antibiotics. In this case we observed an even higher reduction in the dimension of tumor lesions indicating that the spent medium had anti-proliferative activity *in vivo* and this was independent on the microbiota (Figures 5c,d and Extended Data 6b). Furthermore, confirming the observations obtained *in vitro*, the SUP reduced activation of NFATc3 and induced histone H3 acetylation in dysplastic lesions, again in a microbiota-independent fashion (Figure 5e). These data suggest that metabolic products of *F.* PB1 have a direct effect on tumor growth and affect NFATc3 activation.

We then evaluated whether butyrate was sufficient to mediate the anti-proliferative response. We administered sodium butyrate at 1 mM (the same concentration found in the SUP of *F.* PB1) to $Apc^{Min/+}$ mice treated with antibiotics, so to avoid that butyrate could be used up by the indigenous microbiota. As shown in Figures 5f,g butyrate had a very similar antiproliferative activity as *F.* PB1 SUP, indicating that butyrate is the main effector of *F.* PB1 activity.

Finally, we showed that *F.* PB1 SUP significantly reduced the dimension of lesions also in a model of inflammation-driven CRC (AOM/DSS), in which tumors preferentially develop in the colon, more closely mirroring the human pathology (Figures 5h,i and Extended Data 6c).

Overall, these data show that *F.* PB1 metabolic products, in particular butyrate, thanks to their HDACi activity control NFATc3 activation blocking tumor cell proliferation *in vivo* in $Apc^{Min/+}$ mice, independently on the microbiota. A similar antiproliferative activity is observed also in inflammation-driven CRC model.

The anti-proliferative activity of *F.* PB1 can be exerted by other SCFAs producing bacteria.

We then evaluated whether the activity of *F.* PB1 could be shared by other SCFAs producing bacteria. We selected *Lactococcus lactis* because it secreted butyrate and some lactate in culture similarly to *F.* PB1 (Extended Data 7a) and it has been proposed to have anti-proliferative activities *in vitro* by an unknown mechanism[25]. We administered *L. lactis* following a schedule similar to that of *F.* PB1, but we could not detect any anti-tumoral effect (Extended Data 7b,c). This is probably due to the inability of *L. lactis* to survive/colonize in the mouse intestine, as we could not detect *L. lactis* even in WT mice, independently of the microbiota (Extended Data 7d). We

thus analyzed the anti-proliferative activity of SUP from *L. lactis in vivo* in antibiotic treated $Apc^{Min/+}$ mice. We found that the *L. lactis* SUP reduced the size of tumor lesions, even though not as well as *F.* PB1 SUP (Extended Data 7e,f). This difference cannot be due to a reduction in lactate production as lactate did not impact on tumor cell proliferation *in vitro* (Extended Data 7g). Hence, the antiproliferative activity of *F.* PB1 is not unique to this bacterium but can be shared by other bacteria that produce SCFAs as long as they are capable of colonizing or surviving enough time to produce butyrate.

Holdemanella biformis is the equivalent of _F._ PB1 in humans.

We then assessed the relevance of these findings in human CRC. We interrogated a dataset of a shot-gun microbiome analysis carried out in patients with colorectal adenomas[26] and found that, similarly to the mouse, there was a reduction in the abundance of the family of *Erysipelotrichaceae* in patients with large adenomas as compared to healthy individuals, but there was no change in the Shannon diversity index (Figure 6a). In this family, an undefined genus (*Erysipelotrichaceae_noname*) and a species, *Holdemanella biformis*, were strongly underrepresented in advanced colon adenomas (Figure 6b). Interestingly, a high-quality phylogeny of the *Erysipelotrichaceae* family and the *F.* PB1 isolate showed that among the bacteria that colonize the human gut, *Holdemanella biformis* is the second bacterium phylogenetically closest to *F.* PB1 (phylogenetic distance 0.273), as shown in Figure 6c.

H. biformis released SCFAs (Figure 6d), and the SUP of both *F.* PB1 and *H. biformis* inhibited human tumor cell proliferation (HT-29 and Caco-2) (Extended Data 8a) in a comparative way. This activity was mediated by the HDAC inhibitory activity of the

SUP as shown by increased histone acetylation and reduced NFATc3 activation (Figure 6e and Extended Data 8b). I*n vivo,* similarly to *L. lactis*, *H. biformis* was unable to survive/colonize the mouse intestine and we could not observe any anti-proliferative activity in $Apc^{Min/+}$ mice (Extended Data 8c-e). However, when we tested the *H. biformis* SUP in $Apc^{Min/+}$ mice we observed a much higher effect on tumor multiplicity (Figures 6f,g), suggesting that *H. biformis* may have also some effect on tumor initiation. This remains to be evaluated.

We confirmed our data on human specimens from CRC patients using a technology set up in our laboratory[27]. Tumor specimens from CRC patients were treated either with the SCFA mix (acetate:propionate:butyrate 2:1:1) or with the SUP of *F.* PB1 or *H. biformis*. As shown in Figures 6h and Extended Data 9a, SUP of *F.* PB1 or *H. biformis*, as well as the mix of SCFAs induced an increase of H3K27 acetylation and a reduction of NFATc3 protein levels. This correlated with reduced tumor cell proliferation as shown by lower nuclear Ki67 immunostaining in the presence of either *F.* PB1 SUP (Extended Data 9b) or SCFA combination (Extended Data 9c). These results suggest that *H. biformis* is the human counterpart of *F.* PB1.

DISCUSSION

During CRC tumorigenesis, due to epithelial cell dedifferentiation, the mucus layer has been shown to undergo profound changes, both in size and in composition[28]. These changes may result in two concomitant and non-mutually exclusive events that may be responsible for fostering intestinal tumorigenesis. On one side, the increased penetrance or adherence of protumorigenic bacteria which may favor immune cell recruitment and activation, drive tumor cell transformation or Th17 cell activation thus contributing to tumor development[7,29-35]. On the other side, tumorigenesis may be

due to the contraction of anti-tumorigenic bacteria that release anti-proliferative metabolites. We focused on the latter and identified a bacterial member of the murine gut microbiota, *F. rodentium* PB1, belonging to the *Erysipelotrichaceae* family that is one of the most abundant taxa in the murine gut and is not expanded during tumorigenesis, presumably due to the different mucus composition. This may explain why its contraction affects so drastically tumor development.

Tumorigenesis in human CRC and $Apc^{Min/+}$ mice is dependent on a calcineurin-mediated activation of NFATc3 transcription factor which drives tumor cell proliferation[23]. NFATc3 is also involved in driving expression of MUC5ac[36] and this may explain why hCRC and $Apc^{Min/+}$ mice ectopically express MUC5ac. Calcineurin can be induced to degradation by the HDACi panobinostat[24]. Here we show that bacterial spent medium (SUP) from *F.* PB1 and its human counterpart *Holdemanella biformis*, acts as HDACi affecting calcineurin and NFATc3 activation and this results in inhibition of tumor cell growth, independently of the microbiota (Extended Data 10). In some cases we observed an effect of *F.* PB1 or of *H. biformis* SUP also on tumor multiplicity. This could be due to a technical issue due to the inability to detect also small tumors, but we cannot exclude an effect on tumor initiation.

We found a reduction of lactate in the feces of mice treated with *F.* PB1. This was unexpected as *F.* PB1 was found to produce large amounts of lactate *in vitro*, but we cannot anticipate whether it was produced also *in vivo*. In addition, as lactate is known to be produced and used by tumor cells[37,38], we do not know whether the reduction of lactate after *F.* PB1 administration could be due to a reduction of tumor cell proliferation or to an increased use of lactate by tumor cells. Alternatively, lactate could be used by other bacterial species for their own growth[39].

The involvement of SCFAs in the observed anti-proliferative activity is demonstrated by the following observations: 1. evaporation to deplete SCFAs leads to a strong reduction in the activity of the SUP; 2. SUP from another butyrate producing bacterium (*L. lactis*) or 3. butyrate itself, at a concentration similar to that found in the SUP, can mimic the effect of *F.* PB1. This suggests that the anti-tumor activity of *F.* PB1 is not unique and could be shared with other SCFA-producing bacteria as long as they have the ability to colonize or survive in the gut and produce butyrate locally.

Why is butyrate inhibiting proliferation of only tumor cells and not normal epithelial cells? In colorectal cancer, due to the Warburg effect, tumor cells undergo increased glycolysis rather than mitochondrial oxidative metabolism[21]. Thus, cancer cells do not use butyrate for their growth and butyrate concentration raises and can act as HDACi[22]. Consistently, dietary fibers, which promote the growth of butyrate-producing bacteria, affect tumorigenesis in $Apc^{Min/+}$ mice[40] and $Apc^{Min/+}$ mice deleted for *niacr1* (GPR109A, the receptor for butyrate) are more susceptible to tumor development via a mechanism that depends on the microbiota[19].

Consistent with literature data[41,42], we have shown that *Holdemanella biformis* is able to produce SCFAs and its spent medium can inhibit tumor cell proliferation. We do not know whether *H. biformis*, similarly to mouse *F.* PB1, is the major bacterium responsible for the antitumor properties in humans, or whether other SCFA-producing bacteria are also contracted in humans and may contribute to failure of tumor growth control. Future studies should aim at addressing this point and at assessing whether this species may have a therapeutic potential. As *H. biformis* is reduced in the feces of patients with large adenomas, it may also be used as a potential biomarker for detecting tumors in their early phase.

METHODS

Bacterial strains

Faecalibaculum rodentium PB1 was isolated in Kenya Honda laboratory (RIKEN IMS, Yokohama, Japan) from fecal pellets coming from 12 weeks old WT C57BL/6 littermates of our $Apc^{Min/+}$ colony as described in[43]. Briefly, feces were suspended in Tryptic Soy (TS) Broth, serially diluted and plated on Eggerth Gagnon (EG) agar plates. Forty-eight colonies were picked and sequenced using panbacterial primers targeting the 16S rRNA gene. Similarity to *F. rodentium* was checked both on databases and with the sequence retrieved from our metagenomic analysis, resulting in 99.7% and 98% homology respectively. *Holdemanella biformis* was purchased from the German collection of microorganisms DSMZ (Type strain No.: 3989). Both bacteria were cultured in the anaerobic chamber (gas atmosphere $N_2/CO_2/H_2$, 80:15:5), in pre-reduced EG broth under anaerobic conditions for 48 hours. The bacterial strain *Lactococcus lactis* subsp. *lactis* was purchased from DSMZ (Type strain No.:20481) and cultured in pre-reduced MRS broth at 30°C in static conditions. Bacterial supernatant (SUP) was derived from o/n cultures of the strains in the conditions described above. The medium fermented by bacteria (SUP) was filtered in 0,25 μm filters and immediately frozen.

Cell lines

Mouse CRC cell line CT26 and human CRC cell lines HT-29 and Caco-2 were purchased from the American Type Culture Collection (ATCC). CMT-93 mouse rectum carcinoma cell line is a kind gift of Dr. David Artis (Cornell University, NY, USA). MC-38 mouse carcinoma cell line is a kind gift of Dr. Carsten Krieg (Zurich University, Switzerland). APC cell line was derived from $Apc^{Min/+}$ small intestinal

adenomas by mechanical disruption. CT26 cells were cultured in RPMI 1640 supplemented with 10% FBS, 2 mM L-glutamine. CMT-93 and MC-38 cells were cultured in DMEM supplemented with 10% FBS, 2 mM L-glutamine. APC cells were cultured in complete DMEM supplemented with Insulin-Transferrin-Selenium-Ethanolamine (ITS-X, Gibco) and human EGF (10 pg/µl). HT-29 cells were cultured in DMEM supplemented with 10% FBS, 2 mM L-glutamine. Caco-2 were cultured in MEM with Earle's Salt supplemented with 20% FBS, 2 mM L-glutamine, 1 mM sodium pyruvate (NaP), 0.1 mM nonessential amino acids (NEAA). All cell lines were tested to exclude mycoplasma contamination.

To evaluate the effect of SCFA either alone or in combination and of the bacterial spent medium (SUP), cells were seeded and after one overnight stimulated. Cells were stimulated with sodium acetate (S5636, Sigma-Aldrich), sodium propionate (P5436, Sigma Aldrich), sodium butyrate (ARK2161, Sigma-Aldrich) or a mix of the three. APC, CT26, MC-38, HT-29 and Caco-2 cells were stimulated with 50 mM sodium acetate, 10 mM sodium propionate, 2 mM sodium butyrate and a mix of sodium acetate:propionate:butyrate 50:10:2 mM. CMT-93 cells were stimulated with 10 mM sodium acetate, 2.5 mM sodium propionate, 1 mM sodium butyrate and a mix of sodium acetate:propionate:butyrate 10:2.5:1 mM. Cell were stimulated also with different concentrations (0.8, 4, 20 mM) of sodium L-lactate (71718, Sigma-Aldrich). Finally, cells were stimulated with the bacterial broth diluted 40% v/v in cell culture medium, (EG broth) fermented by *F.* PB1 or *H. biformis* (SUP) or relative control non-fermented broth (Vehicle). CT26 cells were treated also with the fermented broth (called also spent medium) evaporated to remove the SCFAs. The spent medium was evaporated to dryness at 50°C under reduced pressure (5 mbar). The residue was taken up with water, filtered and diluted 40% v/v in cell culture medium.

Cell proliferation was evaluated after 48 h of stimulation with CyQUANT Cell Proliferation assay (Molecular Probes). Each condition was tested in 6 wells of a 96-multiwell plate and 12 reads per well were recorded.

Mice

6 weeks old C57BL6/J mice were purchased from Harlan Laboratories. C57BL6/J-Apc^{Min}/J (referred to as $Apc^{Min/+}$ [44]) are maintained as inbred strain in our animal facility. For experiments where $Apc^{Min/+}$ were employed, wild type littermates born from the same mothers of experimental mice were used as controls. All mice were maintained in microisolator cages in specific pathogen-free (SPF) animal facility. Germ-free ICR male mice were maintained in the isolators at RIKEN IMS (Yokohama, Japan). Experiments were performed in accordance with the guidelines established in the Principles of Laboratory Animal Care (directive 86/609/EEC) and approved by the Italian Ministry of Health. On the basis of our experience with animal models and according to animal-welfare policy (directive 86/609/EEC), which strongly suggests the use of a limited number of animals, we estimated that two experiments with n = 5 mice per group would allow us to reach statistical significance. Mice were not randomized. The investigators were not blinded during experimental mice allocation and outcome assessment. For macroscopical analysis of the tumor lesions, we calculated the average of tumor numbers in vehicle group, then the number of tumors of each individual mouse is referred to this average as a percentage.

Bacterial profiling of intestinal microbiota

DNA from fecal pellets and mucus scraped from the small intestine and colon was extracted with G'NOME DNA isolation kit (MP) following a published protocol[45].

476 V5-V6 hypervariable regions of bacterial 16S rRNA gene were amplified and
477 processed with a modified version of the Nextera protocol[46]. Metagenomic libraries
478 obtained were sequenced with MiSeq Illumina platform with 2x250 paired-end (PE)
479 approach. Metagenomic amplicons were analyzed by applying the BioMaS pipeline[47]:
480 (i) the paired-end reads were merged into consensus sequences using PEAR[48] and
481 subsequently dereplicated applying Usearch[49], maintaining the information about the
482 total number of reads supporting each consensus sequence; (ii) the PE reads which
483 remained non overlapping were considered for further analysis only if after the low-
484 quality region trimming (Phred quality cut-off = 25) both read ends were ≥50 bp long;
485 (iii) Both the merged sequences and the unmerged reads were matched against the
486 RDP database (Ribosomal Database Project) (release 11.2)[50] by Bowtie2[51]. The
487 mapping data were filtered according to two parameters: identity percentage and
488 query coverage (≥70%). In particular, sequences obtaining an identity percentage ≥
489 97% were classified to species level and those with identity ≥ 90% and < 97% were
490 classified at higher taxonomic rank; (iv) Finally, all mapped reads fulfilling the settled
491 filters were taxonomically annotated using the Tango tool[52]. Assigned genera were
492 filtered considering as present only the ones for which at least 5 reads per samples
493 were present. The read counts were normalized using an approach similar to the
494 RPKM (Reads per kilo-base per million): normalized count = assigned reads / (total
495 assigned reads at the rank level/1.000.000). Significant differences between WT and
496 $Apc^{Min/+}$ mice in fecal microbiota at the genus and species level were calculated with
497 the DESeq2 R-package[53]. Taxa associated specifically associated to one of the
498 analyzed conditions were identified by using the LEfSe (Linear discriminant analysis
499 Effect Size)[54].

F. PB1 abundance was validated with qPCR assay with specific primers and abundance was normalized to panbacterial primers targeting the 16S rRNA gene (UNI 16S)[55]. Bacterial primer sequences are listed in Table 1.

Normalized reads count for differentially represented species in WT and $Apc^{Min/+}$ mice were log-transformed and plotted as heatmap by using the vegan[56] and the ggplot2[57] R packages.

Histological evaluation

Formalin-fixed and paraffin embedded swiss rolls of colon and small intestine were sectioned at 3-4 mm and the sections stained with hematoxylin and eosin. For histopathological examination and scoring, H&E slides were evaluated by an expert pathologist. The extent of inflammatory changes was defined according to the score proposed by Cooper et al.[58]. The histological scoring system to evaluate the colitis grade is described in Table 2. For each sample, also the number of ulcers and dysplastic/adenomatous lesions was reported. The proliferative lesions are classified according to mouse pathology consensus recommendations[59]. The tissue area of dysplastic and adenomatous lesions was measured on H&E stained slides by digital microscopy. Briefly, slides were digitalized by an Aperio ScanScope CS Slide Scanner (Aperio Technologies) at 40X magnification. The dysplastic and adenomatous lesions were identified and selected using Aperio ImageScope (Leica Biosystems Imaging). The value of every selected dysplastic/adenomatous area is expressed in μm^2 and its major axis in μm.

Fluorescence In situ Hybridization (FISH)

Carnoy's fixed, paraffin embedded tissues were sectioned 5 μm thickness. The probes used were designed to specifically target different regions of the *F.* BPI 16S rRNA. All the probes were manufactured by SIGMA and labelled with Cyanine 3 (5'-[Cy3]GCCAACCAACTAATGCACCG; 5'[CY3]CCGGGAATACGCTCTGGAAA). Probes were used at 5 ng/μl in pre-warmed hybridization buffer (0.9 M NaCl, 20 mM Tris pH 7.4, 0.01% SDS). Slides were incubated at 55°C in a humid chamber for 90 minutes, washed two times at 55°C in pre-warmed washing buffer (0.9 M NaCl, 20 mM Tris pH 7.4), mounted and counterstained with DAPI (contained in the VECTA SHIELD mounting medium). Confocal images were acquired with Leica DMi8 confocal microscope, through HCX PL APO 40X(NA 1.25) oil immersion objective.

Immunofluorescence

In order to maintain the mucus structure, murine intestines were fixed in Carnoy fixative (60% Ethanol, 30% Chloroform, 10% Acetic acid, glacial), manually processed, paraffin embedded and stored at RT until microtome sectioning. Microsections (6 μm thick) were cut using a microtome (Leica), mounted on ultra plus poly-L-lysine-coated glass slides (Menzel-Glaser) and left at 37° o/n. Tissue sections were deparaffinized in histolemon and hydrated through graded alchol series (100%, 95%, 70%, H_2O). Antigen unmasking was performed in Tris-EDTA pH9 (10mM Tris-HCl, 1mM EDTA, Tween 0.05%) for 50 minutes at 95°. Sections were incubated with anti-Muc1 rabbit polyclonal primary antibody (1:100, clone aa 474-630, cat. LS-C343984, LifeSpan Bioscience) at +4° C o/n. After two washing steps in Tris 0.1M pH7.4, slides were incubated with donkey anti-rabbit-Cy3 secondary antibody (1:300, cat. 711165153, Jackson Immuno research) for 2 hours at RT. After washing twice in Tris 0.1M pH7.4 for 10 minutes slides were couterstained and

mounted with VECTASHIELD Mounting Medium with DAPI (Vector Laboratories). Confocal images were acquired with Leica DMi8 confocal microscope through HCX PL APO 40X (NA 1.25) oil immersion objective. All images were adjusted and assembled in Fiji.

RNA extraction, RT–PCR and qPCR

Intestinal chunks from wild type mice, normal ileal chunks and pooled small intestinal polyps from $Apc^{Min/+}$ mice were sampled at 8 and 16 weeks of age. Intestinal tissue was homogenized in 500 µl of TRIzol (Invitrogen). RNA was extracted adding 100 µl of chloroform, precipitating the aqueous phase with 1 volume of 100% ethanol and purifying RNA with *Quick*-RNA MiniPrep Kit (Zymo Research). RNA was retro-transcribed with ImProm-II Reverse Transcriptase kit (Promega). qPCR assay was performed with Fast Sybr Green Master Mix (Life Technologies). Primers used are listed in Table 1. Expression levels are normalized to the 60S ribosomal protein gene expression Rpl32.

Human metagenomics

For the analysis of the Zeller et al. 2014 CRC dataset, raw sequences were downloaded from the sequence read archive (SRA) and used as input into MetaPhlAn2[60]. Individual sample profiles were merged and the final table was filtered to include only members of the *Erysipelotrichaceae* family and samples collected in France. The generated taxonomic profiles are available through the *curatedMetagenomicData* resource[61]. At each taxonomic level, we applied a Wilcoxon Rank-Sum test comparing relative abundances of large adenoma (n = 15) and control samples (n = 61). *P*-values obtained at each taxonomic level were

corrected for multiple hypothesis testing using the Benjamin-Hochberg procedure. A high-quality phylogeny of the *Erysipelotrichaceae* family based on the 400 PhyloPhlAn[62] markers considering 47 complete reference genomes deposited in NCBI (accession ids are reported within brackets in the node labels) and the *F.* PB1 isolate was performed.

Colonic human specimens were obtained from patients diagnosed with colon cancer and undergoing surgery at IEO Inclusion criteria were newly diagnosed CRC patients (stage: I to III), aged between 35-70 years old, performance status 0-1 based on the Eastern Cooperative Oncology Group (ECOG) and signed informed consent according to ICH-GCP. Exclusion criteria were a personal history of malabsorption syndrome or any chronic inflammatory bowel disease, or subjects with hereditary syndrome (such as FAP HNPCC) and use of antibiotics in the previous four weeks. The protocol was approved by the IEO's ethical committee.

_F._ PB1 administration to GF and _F._ PB1, _H. biformis_ and _L. lactis_ administration to $Apc^{Min/+}$ mice

In experiments of gnotobiotic colonization, 5 germ-free ICR male mice were orally administered with 250 µl of *F.* PB1 culture ($O.D._{600nm} \cong 0,6$, corresponding to about 5×10^7 UFC/ml) and the abundance of small intestinal and colonic cells was addressed after 4 weeks. To evaluate the effect of exogenous *F.* PB1 administration, WT and $Apc^{Min/+}$ mice were orally administered 3 times per week with different schedules (see Figures 2d, 2e and 3c) with frozen bacterial stocks equivalent to 250 µl of culture at logarithmic growth phase. At 8, 10 or 12 weeks of age mice were sacrificed and tumor multiplicity in the small intestine and colon assessed. Neutrophil and inflammatory monocyte abundances in circulating blood and Treg, Th1 and Th17

599 abundances in small intestinal and colonic lamina propria were assessed. Bleeding
600 score was assigned as follows: 0 negative to Hemoccult (Beckman Coulter); 1
601 positive to Hemoccult; 2 gross bleeding. To evaluate the effect of exogenous *H.*
602 *biformis* and *L.lactis* administration, $Apc^{Min/+}$ mice were orally administered 3 times
603 per week with frozen bacterial stocks from 8 to 10 weeks of age. In monocolonization
604 experiments, WT and $Apc^{Min/+}$ mice were treated or not with antibiotic cocktail
605 (Ampicillin 1g/L, Neomycin 1g/L, Vancomycin 0.5g/L in drinking water and
606 Metronidazole 2mg/mouse administered by oral gavage every 2 days) for 7 days and
607 challenged with either vehicle or *F.* PB1 or *L.lactis* for 3 days in a row. After 48 h
608 mice were sacrificed and bacterial abundance was validated in the feces, ileal and
609 colon mucus with qPCR assay with specific primers (Table 1).
610
611 **Spent medium (SUP) administration to AOM/DSS treated C57BL6/J WT mice**
612 **or $Apc^{Min/+}$ mice.**
613 8 weeks old C57BL6/J mice were treated with AOM 10mg/Kg of body weight by
614 intraperitoneal injection. After 3 days they received DSS 1.5% w/v in drinking water
615 for 7 days. Mice were allowed for recovery for 14 days. This schedule was repeated
616 for 2 cycles. During the second recovery (from week 12 to 14) AOM/DSS mice were
617 treated by oral gavage (200 µl/mouse) 3 times per week for two weeks with EG broth
618 fermented by *F.* PB1 (*F.* PB1 SUP) or relative control non-fermented broth (Vehicle)
619 and tumor lesions were analyzed.
620 Culture broths fermented with *F.* PB1, *H. biformis* or *L.lactis* (*F.* PB1 SUP, *H.*
621 *biformis* SUP, *L.lactis* SUP) or not (Vehicle) were administered by oral gavage 3
622 times per week for two weeks in 8 weeks old $Apc^{Min/+}$ mice.

623 Vehicle (EG for *F.* PB1 or *H.biformis*; MRS for *L.lactis*), SUP and butyrate 1mM
624 were also administered by oral gavage (200 µl/mouse) 3 times in a row (two times at
625 day 1) in combination with antibiotic cocktail (Ampicillin 1g/L, Neomycin 1g/L,
626 Vancomycin 0.5g/L in drinking water and Metronidazole 2 mg/mouse administered
627 by oral gavage every 2 days) in 11 weeks old $Apc^{Min/+}$ mice pre-treated with antibiotic
628 cocktail for two days. In these experiments mice were sacrificed 24h after the last
629 gavage.
630
631 **Quantification of fecal and spent medium SCFAs**
632 SCFAs were quantified in fecal and spent medium (*F.* PB1 SUP, *H. biformis* SUP and
633 *L. lactis* SUP) samples as previously described[63] with few modifications. In detail,
634 100 mg of feces or 200 µl of SUP were resuspended in 2 ml of 0.001% HCOOH and
635 vortexed for 1 min. The suspension was centrifuged at 1000 x *g* for 2 min at 4 °C and
636 the supernatant was recovered. The residue was extracted again as described above.
637 The supernatants were combined, and the volume was adjusted to 5 ml with a solution
638 of 0.001% HCOOH in water. All extracts were stored at -20 °C. Before UPLC-HR-
639 MS analysis, samples were diluted 1:100 in 0.001% HCOOH and centrifuged at 3000
640 x *g* for 1 min. UPLC-HR-MS analysis was carried out on an Acquity UPLC
641 separation module (Waters, Milford, MA, USA) coupled with an Exactive Orbitrap
642 MS with an HESI-II probe for electrospray ionization (Thermo Scientific, San Jose,
643 CA, USA). The ion source and interface conditions were as follows: spray voltage -
644 3.0 kV, sheath gas flow-rate 35, auxiliary gas-flow rate 10 and temperature 120 °C,
645 and capillary temperature 320 °C. A 1.8-mm HSS T3 column (150 x 2.1 mm, Waters)
646 was used for separation at a flow rate of 0.2 ml/min. The eluents were 0.001%
647 HCOOH in MilliQ-treated water (solvent A) and CH_3OH:CH_3CN (1:1, v/v, solvent

B). A 5 µl aliquot of the sample was separated by the UPLC using the following elution gradient: 0% B for 4 min, 0-15% B in 6 min, 15–20% B in 5 min, 20% for 13 min, and then return to initial conditions in 1 min. The column and samples were maintained at 30 and 15°C, respectively. The UPLC eluate was analyzed in full-scan MS in the range 50–130 *m/z*. The resolution was set at 50 K, the AGC target was 1E6, and the maximum ion injection time was 100 ms. The ion with *m/z* 91.0038, corresponding to the formic acid dimer $[2M-H]^-$, was used as the lock mass. The mass tolerance was 2 ppm. The MS data were processed using Xcalibur software (Thermo Scientific). Analytical grade SCFAs were used as standards (Sigma-Aldrich, Milan, Italy). Five-point external calibration curves were adopted to quantify pyruvic, lactic, succinic, acetic, propionic, butyric, isobutyric, valeric and isovaleric acid in fecal samples. SCFA concentrations were expressed in millimoles per 100 grams of wet feces.

Flow cytometry

Peripheral blood was sampled in heparin and red blood cells were lysed. Samples were stained with CD45.2 PecCP-cy5.5, CD3 PEcy7, Ly6C FITC, Ly6G PE and CD11b APC. On the CD45+ CD3- population neutrophils were defined as Ly6G+ CD11b+ and inflammatory monocytes as $Ly6C^{hi}$ CD11b+.

Small intestinal and colonic lamina propria (LP) lymphocytes were isolated incubating intestinal chunks PBS 5% FCS 1,5 mM EDTA 1mM DTT at 37°C for 15 min to remove epithelial cells. LP cells were mechanically isolated in RPMI 5% FCS with GentleMACS dissociator. T regs were stained FoxP3 intracellular staining kit (eBoscience) with CD45.2 PerCP-cy5.5, CD3 PEcy7, CD4 FITC, CD25 APCcy7, FoxP3 PE and Helios AF647. For Th1 and Th17 detection LP cells were incubated for

4h with PMA (50 ng/ml, Sigma Aldrich), ionomycin (500 ng/ml, Sigma Aldrich) and GolgiStop (BD Biosciences). Cells were then stained with CD45.2 PerCP-cy5.5, CD3 PEcy7, CD4 FITC, CD8 APcy7, IL17 PE, IFNγ APC. Mononuclear phagocytes were stained with CD11b PerCP-Cy5.5 (clone M1/70, BD Biosciences); F4/80 APC (clone BM8, eBioscience); CD11c BV650 (clone N418, Biolegend). Dead cells were excluded with the Fixable Viability Dye eFluor 450 (eBioscience). Samples were acquired at FACSCantoII (BD Biosciences) and analyzed with FlowJo (Treestar).

Western blotting

For western blot analysis cells and tissue samples were lysed with RIPA buffer (50mM Tris-HCl pH 8, 150 mM NaCl, 1mM EDTA, 1% Triton, 1% sodium deoxycholate, 0,1% SDS) supplemented with protease inhibitors (cOmplete Mini, EDTA-free, Roche) and tyrosine protein phosphatases, acid and alkaline-phosphatases inhibitors (Phosphatase Inhibitor Cocktail 2, Sigma-Aldrich) 48h after stimulation and lysates were sonicated. Cell lysates were freshly prepared, measured using Bradford assay (Bio-Rad) and equal amounts of proteins were run on SDS–PAGE and followed by western blotting. After 30 min at room temperature in blocking solution—5% milk or 5% bovine serum albumin (BSA) in tris-buffered saline and Tween-20 (TBST) (10 mM Tris, pH 7.5, 150 mM NaCl, 0.1% (v/v) Tween-20)—membranes were probed with primary antibodies in 5% milk (or 5% BSA) in TBST overnight at 4 °C, washed in TBST and incubated for 1 h at room temperature with secondary antibodies goat anti-rabbit-HRP (1:10,000, 170-6515, Bio-Rad), goat anti-mouse-HRP (1:10,000, 170-6516, Bio-Rad) or rabbit anti-goat-HRP (1:2000, P0449, DAKO). The following primary antibodies were used: anti-PP2B-A (1:1000, clone H-209, sc-9070, Santa Cruz Biotechnology), anti-NFATc3

(1:1000, polyclonal (M-75) sc-8321, monoclonal (F-1) sc-8405, Santa Cruz Biotechnology), anti-Histone H3 acetyl K27 (1:1000, ab4729, abcam), anti-Histone H3 (1:1000, ab1791, abcam), anti-Cytokeratin 18 (1:1000, ab668, abcam), anti-actin (1:1000, A4700, Sigma), anti-Muc1 (1:200, clone F-19, sc-6826, Santa Cruz Biotechnology); anti-Muc13 (1:1000, ab124654, abcam); anti-Muc20 (1:1000, PA5-50238, Thermofisher). Visualization was carried out with chemiluminesence (Clarity Western ECL substrate, Bio-Rad; or ECL, Amersham). Densitometric quantification was performed using ImageJ software.

Immunohistochemistry

Formalin-fixed paraffin embedded sections were deparaffinised and rehydrated through alcohol series. Antigen unmasking was performed in 1 mM EDTA pH 8 for 50 minutes at 95°C. Endogenous peroxidases were quenched with 3% H_2O_2 (SZBF1960V, Sigma). Human slides were incubated with anti-Ki67 antibody (1:200, ab15580, abcam) or anti-NFATc3 polyclonal (1:200, sc-8321, Santa Cruz Biotechnology), whereas mouse slides were incubated with anti-NFATc3 monoclonal (1:200, sc-8405, Santa Cruz Biotechnology, unmasking in EDTA pH8 for 40 minutes at 98 °C) for 2 hours at room temperature. For acetylation visualization antigen unmasking was performed in 10 mM sodium citrate, 0.05% Tween 20, pH 6.0 for 20 minutes at 95°C. After peroxidase quenching slides were incubated 1 hour with anti-Histone H3 acetyl K27 (1:500 for human and 1:800 for mouse tissues ab4729, abcam). After washing slides were incubated with Envision System HRP Rabbit (K4003, DAKO) and developed with DAB solution (K3468, DAKO). Slides were counterstained with hematoxylin and mounted. The DAB+ signal was quantified with ImmunoRatio software[64].

723

724 ***Ex-vivo* stimulation of human colonic mucosa**

725 Colonic human specimens were obtained from patients diagnosed with colon cancer
726 and undergoing surgery at IEO upon informed consent, according to ICH-GCP. The
727 protocol was approved by the IEO's ethical committee. *Ex-vivo* organ cultures were
728 performed on colonic tumor mucosa specimens, according to Tsilingiri et al.[27].
729 Briefly tumor specimens were cut into pieces of about 0.5 cm^2 and placed on sterile
730 metal grids, in a center-well organ culture plate containing 1 ml of medium (DMEM
731 supplemented with 2mM Glutamine, 15% FBS-Na, 1% ITS-X and 200 ng/ml EGF).
732 Tissues were incubated in 100% O_2 atmosphere in the pressure of 1 Atm, inside an
733 airtight container at 37°C, overnight. Colonic tissues were either fixed in 4%
734 paraformaldehyde and processed for histological and IHC analyses or snap-frozen for
735 protein extraction.
736 To evaluate the effect of SCFAs on human colon tumors and controls, medium was
737 supplemented with 200mM sodium acetate (S5636, Sigma-Aldrich), 100mM sodium
738 propionate (P5436, Sigma Aldrich) and 100mM sodium butyrate (ARK2161, Sigma-
739 Aldrich) at a ratio similar to that found in fecal content of *F.* PB1 treated mice
740 (acetate:propionate:butyrate 2:1:1). To evaluate the effect of *F.* PB1 or *H. biformis*-
741 produced SCFAs, fermented EG broth (SUP) was added to the medium at a
742 concentration of 40%; as control, non-fermented EG broth (Veh) was used. Tumor
743 tissues were either processed for immunohistochemistry, or lysed, and H3 acetylation
744 and NFATc3 levels analyzed.
745

746 **Statistical analysis**

747 Data were analyzed for normal distribution before any statistical analyses. Values are
748 presented as means ± standard error mean (SEM) of multiple individual experiments,
749 each of which was carried out at least in triplicate, or as means ± SEM of replicates in
750 a representative experiment. Outliers were detected with the Grubbs' test and
751 excluded from the analysis. The statistical significance between two groups was
752 determined with unpaired Student's *t* test, multiple *t*-tests corrected for multiple
753 comparisons using the Holm-Sidak method, Mann-Whitney test or Wilcoxon Rank-
754 Sum test, whereas the comparison of multiple groups was carried out by Kruskal-
755 Wallis test followed by Dunn test, by one-way or two-way ANOVA, followed by
756 Bonferroni's or Tukey's post-test
757 using GraphPad Prism software (San Diego, CA).
758 The Benjamini and Hochberg procedure was used to adjust *P* values for multiple
759 testing. Data display normal variance. A probability value of $*P < 0.05$ was
760 considered to be significant. No statistical method was used to predetermine
761 sample size. The experiments were not randomized. The investigators were not
762 blinded to allocation during experiments and outcome assessments.
763

764 **Table 1** qPCR primers

Gene	Forward primer (5'→3')	Reverse primer (5'→3')	Amplicon (bp)
Rpl32	AAGCGAAACTGGCGGAAAC	TAACCGATGTTGGGCATCAG	86
Muc1	TACCCTACCTACCACACTCACG	CTGCTACTGCCATTACCTGC	95
Muc3	CTTCCAGCCTTCCCTAAACC	TCCACAGATCCATGCAAAAC	119
Muc5ac	ATCTTTCAGGACCCCTGCTC	ATGGACCACTGGCGTTAGTC	88
Muc13	CAACTCAGCCTTCTGGTGGT	TACAGGGGTTAGGGTTGCAG	90
Muc20	CAACATCTGCATCCACTGCT	GTCAGCCGTACAAGGAGGAA	82
UNI 16S	GGTGAATACGTTCCCGG	TACGGCTACCTTGTTACGACTT	172
F. PB1 16S	CCGGGAATACGCTCTGGAAA	GCCAACCAACTAATGCACCG	123
H. biformis	GCTAAGGCCATGAACATGGA	GCCGTCCTCTTCTGTTCTC	
L. lactis	GCCGTCCTCTTCTGTTCTC	CATTGTGGTTCACCGTTC	

765
766

Table 2 Colitis histological scoring system

Colitis grade	Description
0	Normal colonic mucosa
1	Minimal inflammation restricted to the mucosa and only slightly expanding the lamina propria among crypts or between crypts and *muscularis mucosae*.
2	Mild to moderate (usually focal) inflammation in the mucosa with shortening of the crypts and occasionally mildly extending to the submucosa (usually associated with small ulcers)
3	Moderate to severe (multifocal to diffuse) inflammation involving the mucosa with shortening or loss of the crypts and moderately to markedly extending into the submucosa and occasionally into the *tunica muscularis* (usually associated with large ulcers)
4	Severe transmural inflammation involving the mucosa, submucosa, *tunica muscularis*, and subserosa (usually associated with diffuse ulceration).

DATA AVAILABILITY

The data that support the findings of this study are available from the corresponding author upon request.

REFERENCES

1 Sears, C. L. & Garrett, W. S. Microbes, microbiota, and colon cancer. *Cell host & microbe* **15**, 317-328, doi:10.1016/j.chom.2014.02.007 (2014).

2 Kostic, A. D. *et al.* Genomic analysis identifies association of Fusobacterium with colorectal carcinoma. *Genome research* **22**, 292-298, doi:10.1101/gr.126573.111 (2012).

3 Mima, K. *et al.* Fusobacterium nucleatum in Colorectal Carcinoma Tissue According to Tumor Location. *Clin Transl Gastroenterol* **7**, e200, doi:10.1038/ctg.2016.53 (2016).

783 4 Yu, T. *et al.* Fusobacterium nucleatum Promotes Chemoresistance to
784 Colorectal Cancer by Modulating Autophagy. *Cell* **170**, 548-563 e516,
785 doi:10.1016/j.cell.2017.07.008 (2017).
786 5 Kinzler, K. W. & Vogelstein, B. Lessons from hereditary colorectal cancer.
787 *Cell* **87**, 159-170 (1996).
788 6 Li, Y. *et al.* Gut microbiota accelerate tumor growth via c-jun and STAT3
789 phosphorylation in APCMin/+ mice. *Carcinogenesis* **33**, 1231-1238, doi:bgs137 [pii]
790 10.1093/carcin/bgs137 (2012).
791 7 Kostic, A. D. *et al.* Fusobacterium nucleatum potentiates intestinal
792 tumorigenesis and modulates the tumor-immune microenvironment. *Cell Host*
793 *Microbe* **14**, 207-215, doi:10.1016/j.chom.2013.07.007 (2013).
794 8 Wu, S. *et al.* A human colonic commensal promotes colon tumorigenesis via
795 activation of T helper type 17 T cell responses. *Nat Med* **15**, 1016-1022,
796 doi:10.1038/nm.2015 (2009).
797 9 Arthur, J. C. *et al.* Intestinal inflammation targets cancer-inducing activity of
798 the microbiota. *Science* **338**, 120-123, doi:10.1126/science.1224820 (2012).
799 10 Zhan, Y. *et al.* Gut microbiota protects against gastrointestinal tumorigenesis
800 caused by epithelial injury. *Cancer Res* **73**, 7199-7210, doi:10.1158/0008-5472.CAN-
801 13-0827 (2013).
802 11 Wong, S. H. *et al.* Gavage of Fecal Samples From Patients With Colorectal
803 Cancer Promotes Intestinal Carcinogenesis in Germ-Free and Conventional Mice.
804 *Gastroenterology* **153**, 1621-1633 e1626, doi:10.1053/j.gastro.2017.08.022 (2017).
805 12 Donohoe, D. R. *et al.* A gnotobiotic mouse model demonstrates that dietary
806 fiber protects against colorectal tumorigenesis in a microbiota- and butyrate-

807 dependent manner. *Cancer Discov* **4**, 1387-1397, doi:10.1158/2159-8290.CD-14-
808 0501 (2014).
809 13 Chang, D. H. *et al.* Faecalibaculum rodentium gen. nov., sp. nov., isolated
810 from the faeces of a laboratory mouse. *Antonie Van Leeuwenhoek* **108**, 1309-1318,
811 doi:10.1007/s10482-015-0583-3 (2015).
812 14 Johansson, M. E. *et al.* The inner of the two Muc2 mucin-dependent mucus
813 layers in colon is devoid of bacteria. *Proc Natl Acad Sci U S A* **105**, 15064-15069,
814 doi:0803124105 [pii]
815 10.1073/pnas.0803124105 (2008).
816 15 Xiao, X. *et al.* Role of MUC20 overexpression as a predictor of recurrence
817 and poor outcome in colorectal cancer. *Journal of translational medicine* **11**, 151,
818 doi:10.1186/1479-5876-11-151 (2013).
819 16 Betge, J. *et al.* MUC1, MUC2, MUC5AC, and MUC6 in colorectal cancer:
820 expression profiles and clinical significance. *Virchows Arch* **469**, 255-265,
821 doi:10.1007/s00428-016-1970-5 (2016).
822 17 Guglietta, S. *et al.* Coagulation induced by C3aR-dependent NETosis drives
823 protumorigenic neutrophils during small intestinal tumorigenesis. *Nat Commun* **7**,
824 11037, doi:10.1038/ncomms11037 (2016).
825 18 Sakamoto, M., Tanaka, Y., Benno, Y. & Ohkuma, M. Butyricimonas
826 faecihominis sp. nov. and Butyricimonas paravirosa sp. nov., isolated from human
827 faeces, and emended description of the genus Butyricimonas. *Int J Syst Evol*
828 *Microbiol* **64**, 2992-2997, doi:10.1099/ijs.0.065318-0 (2014).
829 19 Singh, N. *et al.* Activation of gpr109a, receptor for niacin and the commensal
830 metabolite butyrate, suppresses colonic inflammation and carcinogenesis. *Immunity*
831 **40**, 128-139, doi:10.1016/j.immuni.2013.12.007 (2014).

832 20 Boffa, L. C., Vidali, G., Mann, R. S. & Allfrey, V. G. Suppression of histone
833 deacetylation in vivo and in vitro by sodium butyrate. *J Biol Chem* **253**, 3364-3366
834 (1978).
835 21 Vander Heiden, M. G., Cantley, L. C. & Thompson, C. B. Understanding the
836 Warburg effect: the metabolic requirements of cell proliferation. *Science* **324**, 1029-
837 1033, doi:10.1126/science.1160809 (2009).
838 22 Donohoe, D. R. *et al.* The Warburg effect dictates the mechanism of butyrate-
839 mediated histone acetylation and cell proliferation. *Mol Cell* **48**, 612-626,
840 doi:10.1016/j.molcel.2012.08.033 (2012).
841 23 Peuker, K. *et al.* Epithelial calcineurin controls microbiota-dependent
842 intestinal tumor development. *Nat Med* **22**, 506-515, doi:10.1038/nm.4072 (2016).
843 24 Imai, Y. *et al.* Histone deacetylase inhibitor panobinostat induces calcineurin
844 degradation in multiple myeloma. *JCI Insight* **1**, e85061,
845 doi:10.1172/jci.insight.85061 (2016).
846 25 Han, K. J., Lee, N. K., Park, H. & Paik, H. D. Anticancer and Anti-
847 Inflammatory Activity of Probiotic Lactococcus lactis NK34. *J Microbiol Biotechnol*
848 **25**, 1697-1701, doi:10.4014/jmb.1503.03033 (2015).
849 26 Zeller, G. *et al.* Potential of fecal microbiota for early-stage detection of
850 colorectal cancer. *Mol Syst Biol* **10**, 766, doi:10.15252/msb.20145645 (2014).
851 27 Tsilingiri, K., Sonzogni, A., Caprioli, F. & Rescigno, M. A novel method for
852 the culture and polarized stimulation of human intestinal mucosa explants. *Journal of*
853 *visualized experiments : JoVE*, doi:10.3791/4368 (2013).
854 28 Kesari, M. V. *et al.* Immunohistochemical study of MUC1, MUC2 and
855 MUC5AC in colorectal carcinoma and review of literature. *Indian J Gastroenterol* **34**,
856 63-67, doi:10.1007/s12664-015-0534-y (2015).

857 29 Yan, X., Liu, L., Li, H., Qin, H. & Sun, Z. Clinical significance of
858 Fusobacterium nucleatum, epithelial-mesenchymal transition, and cancer stem cell
859 markers in stage III/IV colorectal cancer patients. *Onco Targets Ther* **10**, 5031-5046,
860 doi:10.2147/OTT.S145949 (2017).
861 30 Bullman, S. *et al.* Analysis of Fusobacterium persistence and antibiotic
862 response in colorectal cancer. *Science* **358**, 1443-1448, doi:10.1126/science.aal5240
863 (2017).
864 31 Mendes, R. T. *et al.* Endothelial Cell Response to Fusobacterium nucleatum.
865 *Infect Immun* **84**, 2141-2148, doi:10.1128/IAI.01305-15 (2016).
866 32 Gur, C. *et al.* Binding of the Fap2 protein of Fusobacterium nucleatum to
867 human inhibitory receptor TIGIT protects tumors from immune cell attack. *Immunity*
868 **42**, 344-355, doi:10.1016/j.immuni.2015.01.010 (2015).
869 33 Chen, Y. *et al.* Invasive Fusobacterium nucleatum activates beta-catenin
870 signaling in colorectal cancer via a TLR4/P-PAK1 cascade. *Oncotarget* **8**, 31802-
871 31814, doi:10.18632/oncotarget.15992 (2017).
872 34 Chung, L. *et al.* Bacteroides fragilis Toxin Coordinates a Pro-carcinogenic
873 Inflammatory Cascade via Targeting of Colonic Epithelial Cells. *Cell Host Microbe*,
874 doi:10.1016/j.chom.2018.01.007 (2018).
875 35 Dejea, C. M. *et al.* Patients with familial adenomatous polyposis harbor
876 colonic biofilms containing tumorigenic bacteria. *Science* **359**, 592-597,
877 doi:10.1126/science.aah3648 (2018).
878 36 Yan, F. *et al.* Interleukin-13-induced MUC5AC expression is regulated by a
879 PI3K-NFAT3 pathway in mouse tracheal epithelial cells. *Biochem Biophys Res*
880 *Commun* **446**, 49-53, doi:10.1016/j.bbrc.2014.02.051 (2014).

881 37 San-Millan, I. & Brooks, G. A. Reexamining cancer metabolism: lactate
882 production for carcinogenesis could be the purpose and explanation of the Warburg
883 Effect. *Carcinogenesis* **38**, 119-133, doi:10.1093/carcin/bgw127 (2017).
884 38 Faubert, B. *et al.* Lactate Metabolism in Human Lung Tumors. *Cell* **171**, 358-
885 371 e359, doi:10.1016/j.cell.2017.09.019 (2017).
886 39 Duncan, S. H., Louis, P. & Flint, H. J. Lactate-utilizing bacteria, isolated from
887 human feces, that produce butyrate as a major fermentation product. *Appl Environ*
888 *Microbiol* **70**, 5810-5817, doi:10.1128/AEM.70.10.5810-5817.2004 (2004).
889 40 Donohoe, D. R. *et al.* A gnotobiotic mouse model demonstrates that dietary
890 fiber protects against colorectal tumorigenesis in a microbiota- and butyrate-
891 dependent manner. *Cancer discovery* **4**, 1387-1397, doi:10.1158/2159-8290.CD-14-
892 0501 (2014).
893 41 Zhernakova, A. *et al.* Population-based metagenomics analysis reveals
894 markers for gut microbiome composition and diversity. *Science* **352**, 565-569,
895 doi:10.1126/science.aad3369 (2016).
896 42 De Maesschalck, C. *et al.* Faecalicoccus acidiformans gen. nov., sp. nov.,
897 isolated from the chicken caecum, and reclassification of Streptococcus pleomorphus
898 (Barnes et al. 1977), Eubacterium biforme (Eggerth 1935) and Eubacterium
899 cylindroides (Cato et al. 1974) as Faecalicoccus pleomorphus comb. nov.,
900 Holdemanella biformis gen. nov., comb. nov. and Faecalitalea cylindroides gen. nov.,
901 comb. nov., respectively, within the family Erysipelotrichaceae. *Int J Syst Evol*
902 *Microbiol* **64**, 3877-3884, doi:10.1099/ijs.0.064626-0 (2014).
903 43 Atarashi, K. *et al.* Treg induction by a rationally selected mixture of Clostridia
904 strains from the human microbiota. *Nature* **500**, 232-236, doi:10.1038/nature12331
905 (2013).

906 44 Moser, A. R., Pitot, H. C. & Dove, W. F. A dominant mutation that
907 predisposes to multiple intestinal neoplasia in the mouse. *Science* **247**, 322-324
908 (1990).
909 45 Furet, J. P. *et al.* Comparative assessment of human and farm animal faecal
910 microbiota using real-time quantitative PCR. *FEMS Microbiol Ecol* **68**, 351-362,
911 doi:10.1111/j.1574-6941.2009.00671.x (2009).
912 46 Manzari, C. *et al.* Draft genome sequence of Sphingobium sp. strain ba1,
913 resistant to kanamycin and nickel ions. *FEMS Microbiol Lett* **361**, 8-9,
914 doi:10.1111/1574-6968.12618 (2014).
915 47 Fosso, B. *et al.* BioMaS: a modular pipeline for Bioinformatic analysis of
916 Metagenomic AmpliconS. *BMC Bioinformatics* **16**, 203, doi:10.1186/s12859-015-
917 0595-z (2015).
918 48 Zhang, J., Kobert, K., Flouri, T. & Stamatakis, A. PEAR: a fast and accurate
919 Illumina Paired-End reAd mergeR. *Bioinformatics* **30**, 614-620,
920 doi:10.1093/bioinformatics/btt593 (2014).
921 49 Edgar, R. C. Search and clustering orders of magnitude faster than BLAST.
922 *Bioinformatics* **26**, 2460-2461, doi:10.1093/bioinformatics/btq461 (2010).
923 50 Cole, J. R. *et al.* The Ribosomal Database Project: improved alignments and
924 new tools for rRNA analysis. *Nucleic Acids Res* **37**, D141-145,
925 doi:10.1093/nar/gkn879 (2009).
926 51 Langmead, B. & Salzberg, S. L. Fast gapped-read alignment with Bowtie 2.
927 *Nat Methods* **9**, 357-359, doi:10.1038/nmeth.1923 (2012).
928 52 Alonso-Alemany, D. *et al.* Further steps in TANGO: improved taxonomic
929 assignment in metagenomics. *Bioinformatics* **30**, 17-23,
930 doi:10.1093/bioinformatics/btt256 (2014).

931 53 Love, M. I., Huber, W. & Anders, S. Moderated estimation of fold change and
932 dispersion for RNA-seq data with DESeq2. *Genome Biol* **15**, 550,
933 doi:10.1186/s13059-014-0550-8 (2014).
934 54 Segata, N. *et al.* Metagenomic biomarker discovery and explanation. *Genome*
935 *Biol* **12**, R60, doi:10.1186/gb-2011-12-6-r60 (2011).
936 55 Salzman, N. H. *et al.* Enteric salmonella infection inhibits Paneth cell
937 antimicrobial peptide expression. *Infect Immun* **71**, 1109-1115 (2003).
938 56 Oksanen, J. *et al.* vegan: community ecology package. R package vegan, vers.
939 2.2-1. (2015).
940 57 Wickham, H. Ggplot2: Elegant Graphics for Data Analysis. *Springer, New*
941 *York*, VIII, 213 (2009).
942 58 Cooper, H. S., Murthy, S. N., Shah, R. S. & Sedergran, D. J. Clinicopathologic
943 study of dextran sulfate sodium experimental murine colitis. *Lab Invest* **69**, 238-249
944 (1993).
945 59 Boivin, G. P. *et al.* Pathology of mouse models of intestinal cancer: consensus
946 report and recommendations. *Gastroenterology* **124**, 762-777,
947 doi:10.1053/gast.2003.50094 (2003).
948 60 Truong, D. T. *et al.* MetaPhlAn2 for enhanced metagenomic taxonomic
949 profiling. *Nat Methods* **12**, 902-903, doi:10.1038/nmeth.3589 (2015).
950 61 Pasolli, E. *et al.* Accessible, curated metagenomic data through
951 ExperimentHub. *Nat Methods* **14**, 1023-1024, doi:10.1038/nmeth.4468 (2017).
952 62 Segata, N., Bornigen, D., Morgan, X. C. & Huttenhower, C. PhyloPhlAn is a
953 new method for improved phylogenetic and taxonomic placement of microbes. *Nat*
954 *Commun* **4**, 2304, doi:10.1038/ncomms3304 (2013).

63 Gargari, G. *et al.* Consumption of a Bifidobacterium bifidum Strain for 4 Weeks Modulates Dominant Intestinal Bacterial Taxa and Fecal Butyrate in Healthy Adults. *Appl Environ Microbiol* **82**, 5850-5859, doi:10.1128/AEM.01753-16 (2016).

64 Tuominen, V. J., Ruotoistenmaki, S., Viitanen, A., Jumppanen, M. & Isola, J. ImmunoRatio: a publicly available web application for quantitative image analysis of estrogen receptor (ER), progesterone receptor (PR), and Ki-67. *Breast Cancer Res* **12**, R56, doi:10.1186/bcr2615 (2010).

ACKNOWLEDGEMENTS

We thank Mattia Bugatti and Sara Licini (supported by Fondazione Beretta, Brescia, Italy) for technical support in histological analysis; Andrew Thomas and Edoardo Pasolli for performing bioinformatics analyses; Cristina Faccani for technical support in *in vitro* experiments; Erika Mileti, Claudia Burrello and Maria Rita Giuffré for technical support in *in vivo* experiments. **Funding**: this work has been supported by grants of the Italian Association for Cancer Research (AIRC) and the European Research council (ERC) to M.R., E.Z. was a recipient of a FIRC fellowship. TS is a recipient of a fellowship from Fondazione Veronesi.

AUTHORS CONTRIBUTIONS

E.Z. and C.P. ideated, performed and analysed all the experiments; T.S. and F.S. helped in the execution of experiments; A.B., I.S. and Sil.G. helped in the execution of the mouse experiments; B.F., M.M. and Gr.P. performed 16s rRNA metagenomic analysis; L.M. and W.V. designed and carried out histological analyses. G.N. performed ex-vivo stimulation of human colonic mucosa experiments; A.B. performed confocal analyses; J.T. executed metabolomic analyses; B.O. helped in the

execution of *in vitro* experiments; K.A. and K.H. isolated F.PB1 and carried out GF experiments; S.A. and S.G. set up *F.* PB1 growth and supernatant production; S.C. set up *H. biformis* and *L. lactis* growth and supernatant production; G.F. performed FACS analyses; F.A. and N.S. performed phylogenetic analysis and human CRC dataset interrogation; G.P. participated with ideas and results interpretation; M.R. ideated the study, coordinated the work, and wrote the manuscript.

DECLARATION OF INTERESTS

The authors declare no competing interests.

FIGURE LEGENDS

Figure 1. *Faecalibaculum rodentium* is underrepresented during the early phases of tumor development

(a-c) 16S rRNA gene profiling of the fecal microbiota of WT and $Apc^{Min/+}$ mice at 4, 8 and 12 weeks of age. (a) Shannon diversity index. Box plots show median value and whiskers min to max. (b) Genus abundance (inner pie: WT, outer pie: $Apc^{Min/+}$). Genera with a relative abundance higher than 1% in at least one of the tested condition, were shown, otherwise are collapsed into the "Other genera" section. Significance assessed by Mann-Whitney test. (c) Relative abundance of the 10 most abundant species in fecal bacterial DNA of WT mice isolated from WT and $Apc^{Min/+}$ mice at 8 and 12 weeks of age. Abundance shown as the normalized number of assigned sequences in the 16S rRNA sequencing. Significance determined by two-way ANOVA with Bonferroni post-test. (d,e) qPCR of *F.* PB1 abundance normalized to panbacterial primers targeting the 16S rRNA gene (UNI 16S) in bacterial DNA extracted from feces (d) and mucus from the small intestine and colon (e) from WT

and $Apc^{Min/+}$ mice. Significance determined by multiple *t*-tests corrected for multiple comparisons using the Holm-Sidak method (d) to compare *F.* PB1 abundance between groups at each time point or by unpaired *t*-test (e).

Data from two independent experiments (n = 7−8 mice/group, a-d; n = 11 mice/group, e) and represented as means ± SEM. ***P* <0.01; ****P* <0.001; *****P* <0.0001.

Figure 2. *F.* PB1 loss coincides with mucus changes and when reintroduced reduces tumor growth

(a) qPCR of mucin expression in the ileal tissue of WT mice and healthy (H) and tumor (T) tissue of $Apc^{Min/+}$ mice at 8 and 16 weeks of age. Expression levels are normalized to the reference gene Rpl32. Data from two independent experiments (n = 7−10 mice/group). Significance determined by one-way ANOVA with Bonferroni post-test to compare expression levels within the same time point. (b,c) *F.* PB1 administration experiments in WT and $Apc^{Min/+}$ mice pre-treated with antibiotic cocktail. (b) qPCR of *F.* PB1 abundance normalized to panbacterial primers targeting the 16S rRNA gene (UNI 16S) in bacterial DNA extracted from ileal mucus. Data from two independent experiments (WT n = 6−7, $Apc^{Min/+}$ n = 10−11 mice/group). Significance determined by Mann-Whitney test. (c) Representative FISH images of *F.* PB1 (green) on the mucosal surface of $Apc^{Min/+}$ ileum polyp and WT normal ileum. DAPI nuclear stain in blue. Images obtained at 40X magnification; n = 3 mice/group. (d) Tumor multiplicity in the small intestine of $Apc^{Min/+}$ mice treated with vehicle (Veh) or *F.* PB1 from week 4 to 8 (n = 5 mice/group). Significance determined by multiple *t*-tests corrected for multiple comparisons using the Holm-Sidak method to compare tumor multiplycity between groups at each time point.

(e,f) $Apc^{Min/+}$ mice received vehicle (Veh) or *F.* PB1 from week 8 to 12. (e) Tumor multiplicity in the small intestine normalized to vehicle treated $Apc^{Min/+}$ mice at 12 weeks of age. Data from two independent experiments depicted (n = 13–14 mice/group). (f) Area and maximum diameter (axis length) of ileal dysplastic lesions normalized to the total number of lesions per mouse. Box plots show median value and whiskers min to max. Significance determined by unpaired *t*-test (e) and Mann-Whitney test (f). Data are represented as means ± SEM. **P* <0.05; ***P* <0.01; ****P* <0.001; *****P* <0.0001.

Figure 3. *F.* PB1 reduces tumor cell proliferation without major impact on immune cells

(a,b) WT and $Apc^{Min/+}$ mice treated with vehicle (Veh) or *F.* PB1 from week 8 to 12. (a) Flow cytometric analysis of T regulatory, Th1 and Th17 cell populations in the small intestinal lamina propria. FoxP3+CD25+ are gated on the live CD45+ CD3+ CD4+ cells; Helios+ is gated on the FoxP3+ CD25+ cells. IL17+, IFNγ+ and IL17+ IFNγ+ cells are gated on the live CD45+ CD3+ CD4+ cells; n = 8–10 mice/group.

(b) Flow cytometric analysis of peripheral blood cells. Percentages are relative to the CD45+ CD3- population; n = 12–15 mice/group. (c-g) $Apc^{Min/+}$ mice received vehicle (Veh) or *F.* PB1 from week 8 to 10. Mice from two independent experiments depicted (n = 10–11 mice/group). (c) Tumor multiplicity in the small intestine normalized to vehicle treated $Apc^{Min/+}$ mice. (d) Area and maximum diameter (axis length) of ileal dysplastic lesions (number of lesions is indicated) normalized to the total number of lesions per mouse. Box plots show median value and whiskers min to max. (e) Percentage of nuclear Ki67 positive cells in the polyps of vehicle and *F.* PB1-treated mice; n = 4 mice/group, polyps n = 9–33. (f) Representative images of nuclear Ki67

staining in polyps of vehicle and *F.* PB1-treated mice. n = 4 mice/group. (g) Bleeding score of vehicle and *F.* PB1-treated mice. (h) Fecal concentrations of L-lactate, acetate, propionate and butyrate in WT and $Apc^{Min/+}$ mice treated with vehicle or *F.* PB1 from 8 to 12 weeks, detected by UPLC-MS; n = 5−11 mice/group.

Data are represented as means ±SEM, and represent the pool of two or three independent experiments. **P* <0.05; ***P* <0.01; ****P* <0.001, *****P* <0.0001. Significance assessed by one-way ANOVA using Bonferroni post-test for multiple comparisons (a) or unpaired *t*-test (b,c,e,g,), Mann-Whitney test (d), or two-way ANOVA with Bonferroni post-test for multiple comparisons (h).

Figure 4. *F.* PB1 releases SCFAs that have anti-proliferative activity

(a,c) Cell proliferation assay on mouse CRC cell lines treated or not (NT) with acetate (Ac), propionate (Prop) and butyrate (But) either alone and in combination (MIX) (a) or with culture broth fermented by *F.* PB1 (SUP) (c). t0 is the signal from cells at the time of stimulation. Data of a representative experiment are reported. * indicates comparison with NT, # represents comparison with the MIX, ° represents comparison with the t0. Significance determined by one-way ANOVA using Bonferroni post-test. (b) Quantification of L-lactate and SCFAs in broth fermented by *F.* PB1 (SUP) by UPLC-MS. Data from six independent experiments. (d) Representative Western blots from two to three independent experiments showing the effect on H3K27 acetylation, PP2B-A and NFATc3 expression in mouse cell lines treated or not (NT) with broths fermented by *F.* PB1 (SUP) or not fermented (Veh). Vinculin and actin used as loading controls. Dentitometric analysis is reported in Extended Data 5b. (e,f) *In vitro* stimulation of CT26 cells with untreated broth fermented by *F.* PB1 (SUP) or one depleted of SCFAs by evaporation (SUP evap). Untreated broth not fermented (Veh)

or evaporated (Veh evap) used as a controls. (e) Representative Western blots from two independent experiments showing the effect of SUP and SUP evap on H3K27 acetylation and NFATc3 expression. Vinculin was used as loading controls. Densitometric analysis is reported in Extended Data 5c. (f) Quantification of SCFAs and L-lactate by UPLC-MS. Data from three independent experiments. Significance determined by Mann-Whitney test. Data are represented as means ± SEM. *P <0.05; ### and ***P <0.001; ####, °°°° and ****P <0.0001.

Figure 5. *F.* PB1 metabolic products, in particular butyrate, have anti-proliferative activity *in vivo* and this is independent on the microbiota

(a,b) $Apc^{Min/+}$ mice received broths not fermented (Veh) or fermented by *F.* PB1 (SUP) from week 8 to 10. Data from three independent experiments depicted (n = 11−13 mice/group). (c-e) 11 weeks old $Apc^{Min/+}$ mice treated with Veh or *F.* PB1 SUP in the presence of an antibiotic cocktail (ABX). Data from two independent experiments depicted (n = 6−7 mice/group). (f,g) 11 weeks old $Apc^{Min/+}$ mice treated with Veh, *F.* PB1 SUP or butyrate 1 mM in the presence of ABX. Mice from two independent experiments depicted (n = 4 mice/group). (a,c,f) Tumor multiplicity in the small intestine normalized to vehicle treated $Apc^{Min/+}$ mice. (b,d,g) Area and maximum diameter of ileal dysplastic lesions normalized to the total number lesions per mouse. (e) Representative images of ileal dysplastic lesions stained with anti-NFATc3 antibody (200X magnification, scale bar 100 μm) or with anti-Histone H3 acetyl K27 antibody (100X magnification, scale bar 200 μm). Observations from n = 11−14 dysplastic lesions. Right panel: Quantitative color deconvolution analysis of Histone H3 acetylation in dysplastic lesions of $Apc^{Min/+}$ mice treated or not with *F.* PB1 SUP. (h,i) AOM/DSS treated C57BL/6 WT mice received Veh or *F.* PB1 SUP (n

= 5–6 mice/group). (h) Tumor multiplicity in the colon normalized to vehicle treated $Apc^{Min/+}$. (i) Area and maximum diameter (axis length) of colon adenomas.

Data are represented as means ± SEM and box plots show median value and whiskers min to max. *P <0.05; **P <0.01; ***P <0.001. Significance was evaluated using Mann Whitney test (a-e,h), Kruskal-Wallis test with Dunn post-test (f,g) or unpaired *t*-test (i).

Figure 6. *Holdemanella biformis* is the equivalent of *F.* PB1 in humans

(a) Shannon diversity index in fecal DNA from healthy donors and large adenoma patients and abundance of the family *Erysipelotrichaceae*. (b) Abundance of the undefined genus *Erysipelotrichaceae noname* and of the species *Holdemanella biformis*. At each taxonomic level, a Wilcoxon Rank-Sum test comparing relative abundances of large adenoma (n = 15) and control samples (n = 61) was applied. *P*-values obtained at family and genus taxonomic levels were corrected for multiple hypothesis testing using the Benjamin-Hochberg procedure. (c) A high-quality phylogeny of the *Erysipelotrichaceae* family and the *F.* PB1 isolate. (d) Quantification of SCFAs in the broth fermented by *Holdemanella biformis* (*H. biformis* SUP) by UPLC-MS. Data from two independent experiments. (e) Representative WB showing the effect of SCFAs MIX, *F.* PB1 SUP, *H. biformis* SUP on H3K27 acetylation and NFATc3 expression in human CRC cell lines. Cells not treated (NT) or treated with non-fermented medium (Veh) as a control. Vinculin used as loading control. Densitometric analysis is reported in Extended Data 8b. (f,g) 11 weeks old $Apc^{Min/+}$ mice treated with Veh or *H. biformis* SUP in the presence of antibiotics (ABX) (n = 5 mice/group). (f) Tumor multiplicity in the small intestine normalized to vehicle treated $Apc^{Min/+}$ mice. (g) Area and maximum diameter of ileal

dysplastic lesions normalized to the total number lesions per mouse. (h) Representative WB showing the effect of *F.* PB1 SUP or *H. biformis* SUP on H3K27 acetylation and NFATc3 expression in *ex-vivo* treated human colon tumor samples (hCRC). Right panels show the densitometric quantification of NFATc3 (normalized to vinculin) and H3K27 acetylation (normalized to total H3) from one, two or three independent experiments.

Data are represented as means ± SEM and box plots show median value and whiskers min to max. **P* <0.05; ***P* <0.01; ****P* <0.001. Significance was evaluated using Mann Whitney test (f,g) and unpaired *t*-test (h).

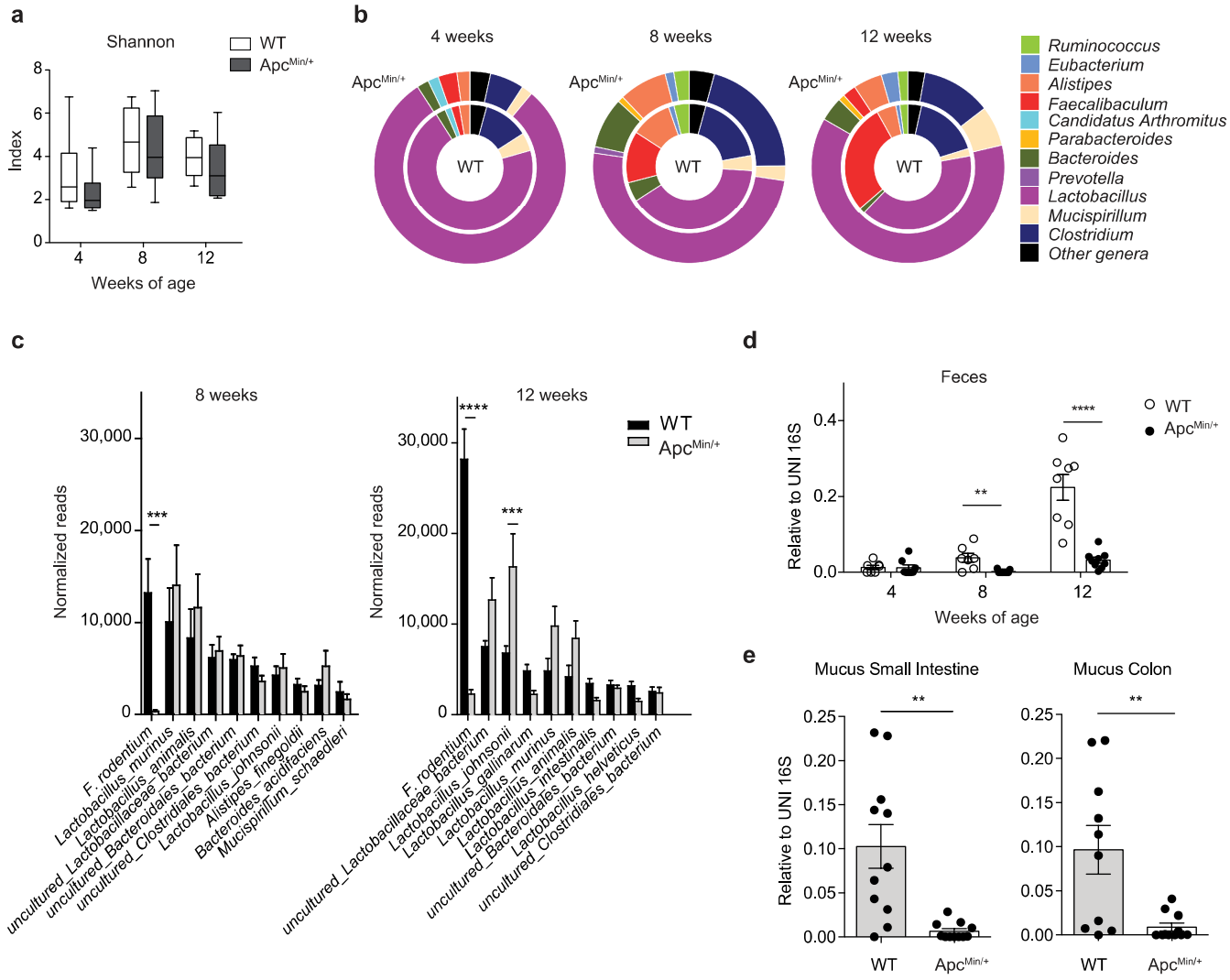
a
Shannon
WT
Apc^Min/+
Index
Weeks of age
b
4 weeks
8 weeks
12 weeks
Apc^Min/+
WT
Ruminococcus
Eubacterium
Alistipes
Faecalibaculum
Candidatus Arthromitus
Parabacteroides
Bacteroides
Prevotella
Lactobacillus
Mucispirillum
Clostridium
Other genera
c
8 weeks
12 weeks
Normalized reads
WT
Apc^Min/+
F. rodentium
Lactobacillus_murinus
Lactobacillus_animalis
uncultured_Lactobacillaceae_bacterium
uncultured_Bacteroidales_bacterium
uncultured_Clostridiales_bacterium
Lactobacillus_johnsonii
Alistipes_finegoldii
Bacteroides_acidifaciens
Mucispirillum_schaedleri
Lactobacillus_gallinarum
d
Feces
Relative to UNI 16S
Weeks of age
e
Mucus Small Intestine
Mucus Colon
Relative to UNI 16S

Figure 1

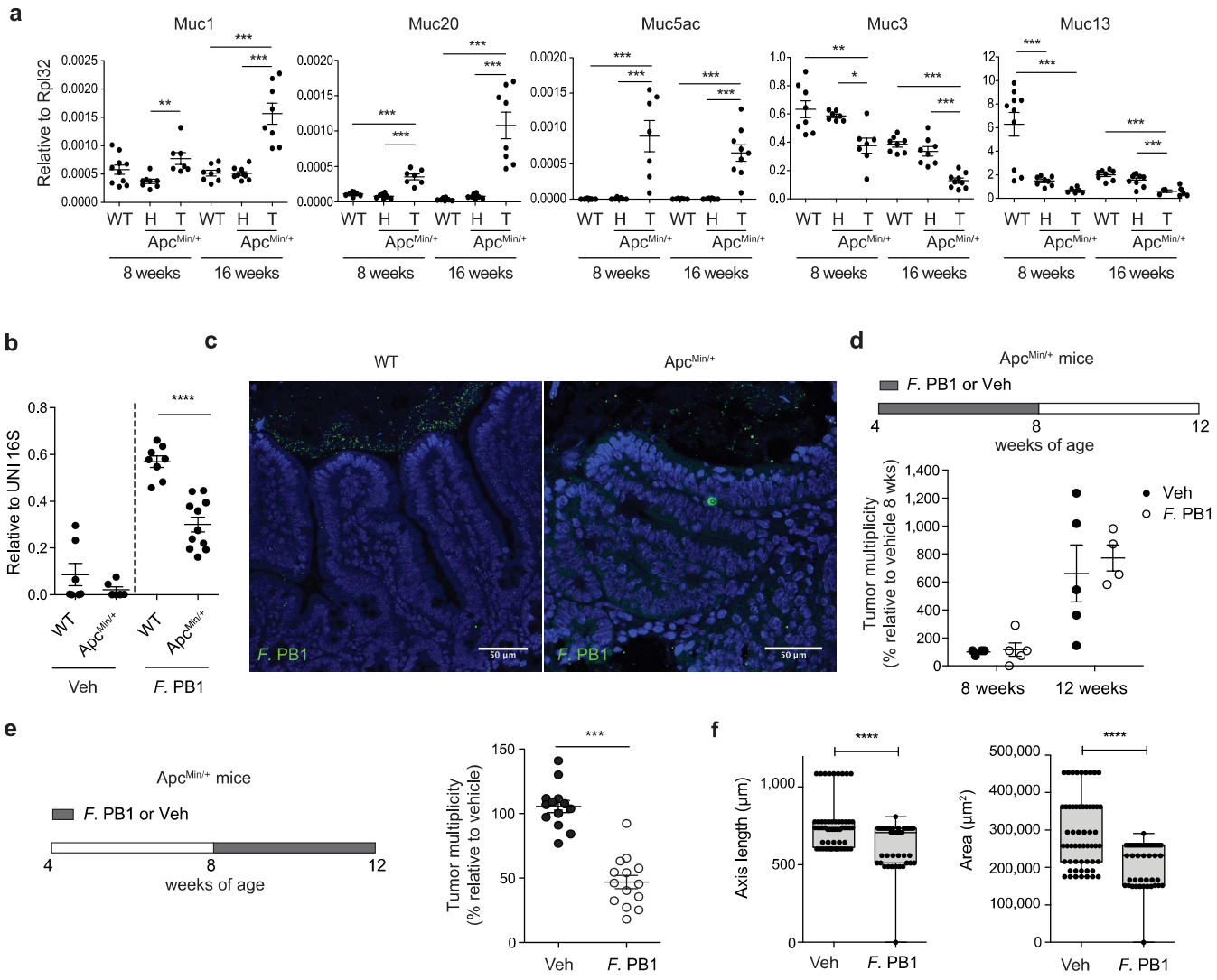
a
Muc1
Muc20
Muc5ac
Muc3
Muc13
Relative to Rpl32
WT H T WT H T
ApcMin/+
8 weeks
16 weeks
b
Relative to UNI 16S
Veh
F. PB1
c
WT
ApcMin/+
F. PB1
50 µm
d
ApcMin/+ mice
F. PB1 or Veh
weeks of age
Tumor multiplicity
(% relative to vehicle 8 wks)
Veh
F. PB1
8 weeks
12 weeks
e
ApcMin/+ mice
F. PB1 or Veh
weeks of age
Tumor multiplicity
(% relative to vehicle)
f
Axis length (µm)
Area (µm²)

Figure 2

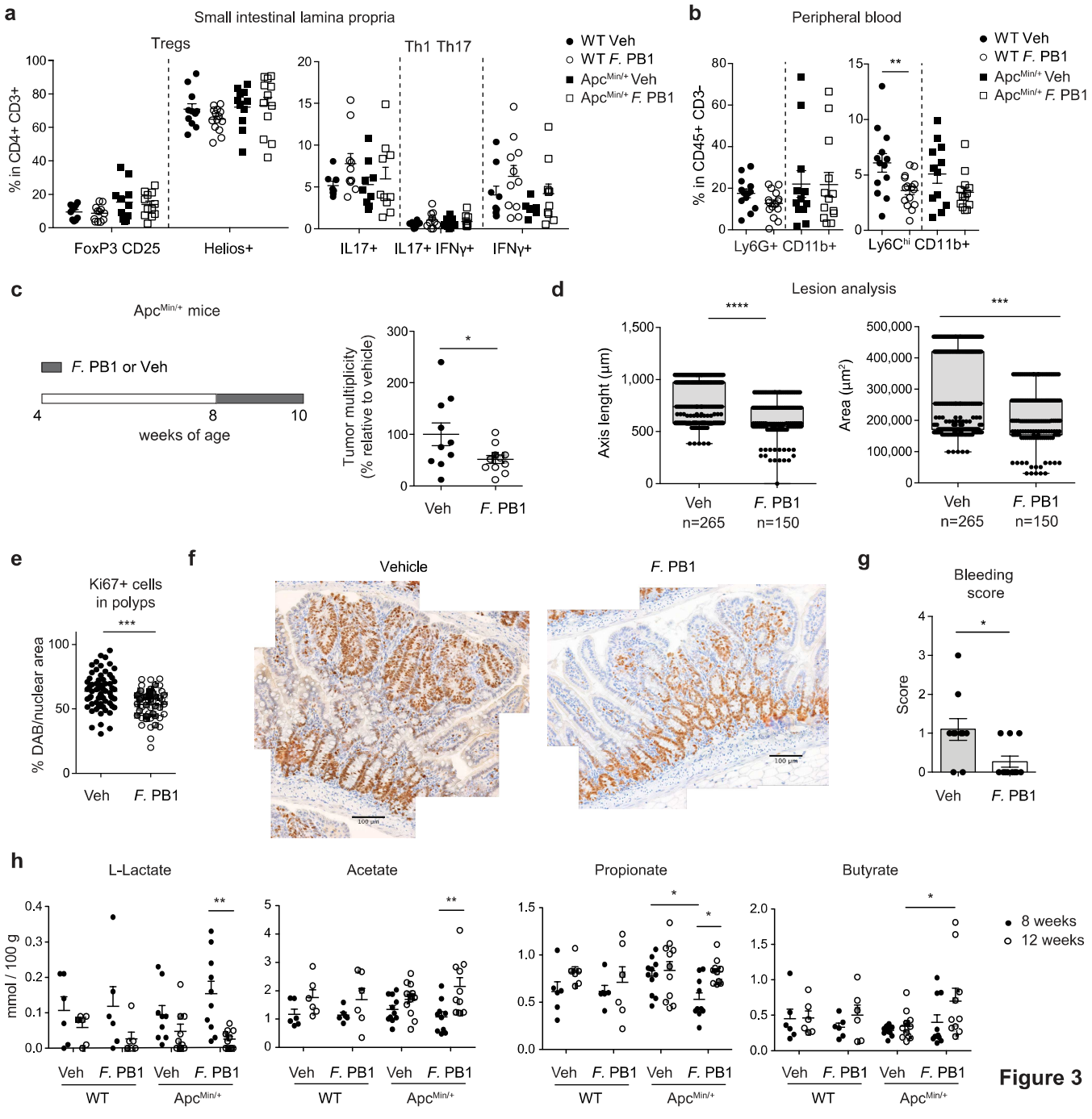
a
Small intestinal lamina propria
Tregs
Th1 Th17
% in CD4+ CD3+
FoxP3 CD25
Helios+
IL17+
IL17+ IFNγ+
IFNγ+
WT Veh
WT F. PB1
Apc Min/+ Veh
Apc Min/+ F. PB1
b
Peripheral blood
% in CD45+ CD3-
Ly6G+ CD11b+
Ly6C hi CD11b+
c
Apc Min/+ mice
F. PB1 or Veh
4
8
10
weeks of age
Tumor multiplicity (% relative to vehicle)
Veh
F. PB1
d
Lesion analysis
Axis lenght (µm)
Area (µm²)
Veh n=265
F. PB1 n=150
e
Ki67+ cells in polyps
% DAB/nuclear area
f
Vehicle
F. PB1
g
Bleeding score
Score
h
L-Lactate
Acetate
Propionate
Butyrate
mmol / 100 g
WT
Apc Min/+
8 weeks
12 weeks

Figure 3

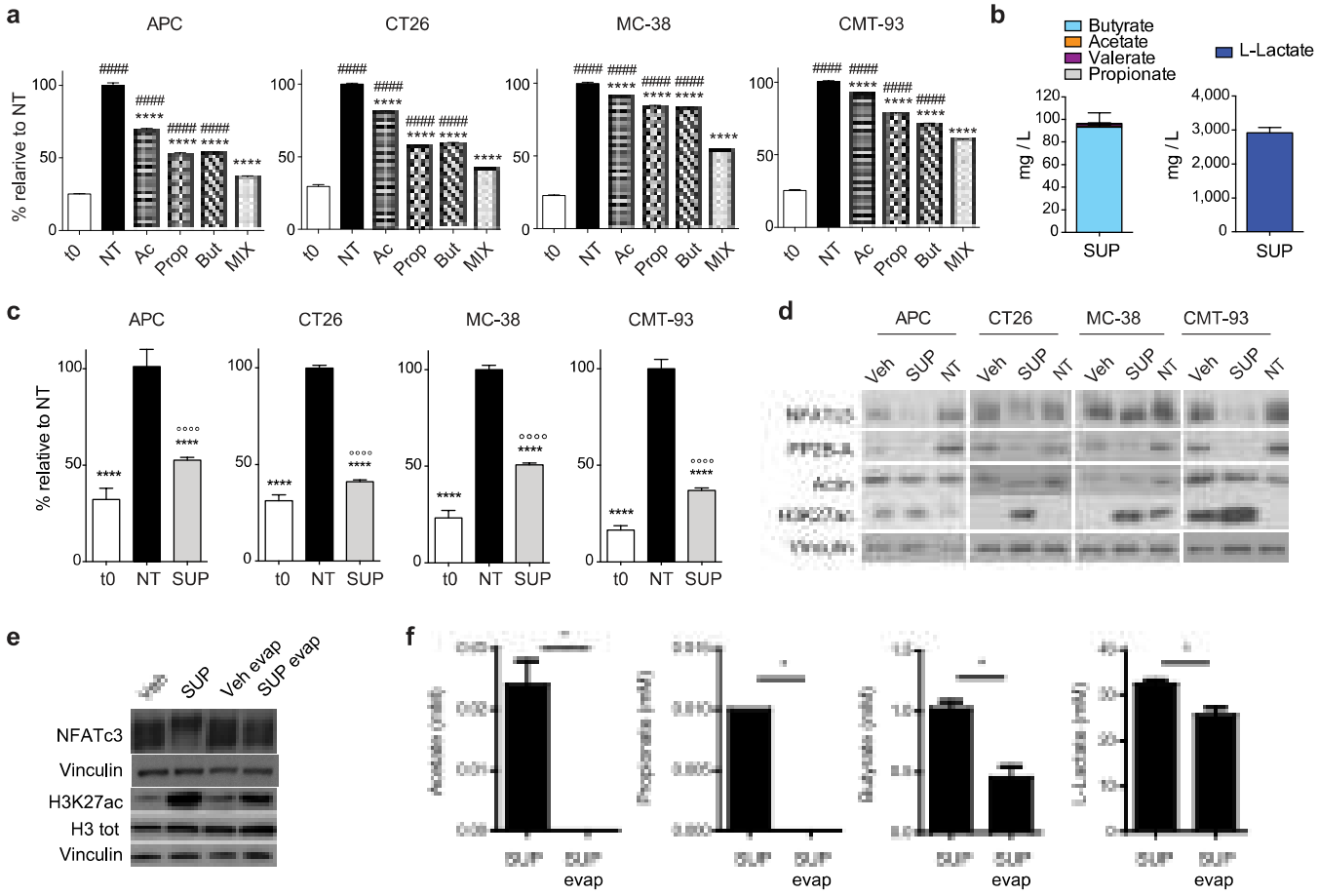
a
APC
CT26
MC-38
CMT-93
% relarive to NT
t0
NT
Ac
Prop
But
MIX
b
Butyrate
Acetate
Valerate
Propionate
L-Lactate
mg /L
SUP
c
% relative to NT
t0
NT
SUP
d
APC
CT26
MC-38
CMT-93
Veh
SUP
NT
e
SUP
Veh evap
SUP evap
NFATc3
Vinculin
H3K27ac
H3 tot
Vinculin
f
SUP
SUP evap

Figure 4

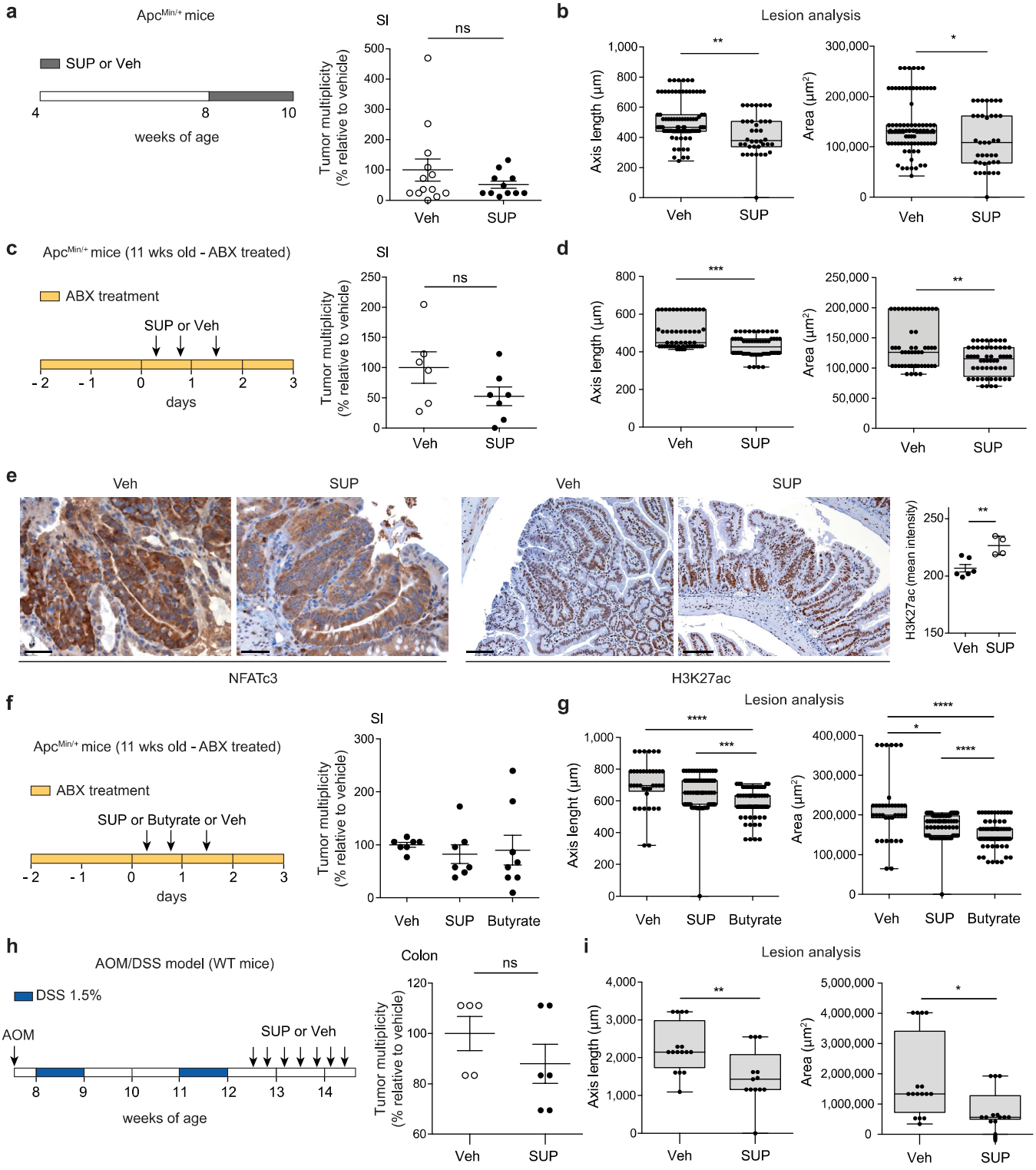
a
Apc^Min/+ mice
SUP or Veh
4
8
10
weeks of age
SI
ns
Tumor multiplicity (% relative to vehicle)
Veh
SUP
b
Lesion analysis
Axis length (µm)
Area (µm²)
**
*
Veh
SUP
c
Apc^Min/+ mice (11 wks old - ABX treated)
ABX treatment
SUP or Veh
-2
-1
0
1
2
3
days
SI
ns
Tumor multiplicity (% relative to vehicle)
Veh
SUP
d
Axis length (µm)
Area (µm²)
***
**
Veh
SUP
e
Veh
SUP
Veh
SUP
NFATc3
H3K27ac
H3K27ac (mean intensity)
**
Veh
SUP
f
Apc^Min/+ mice (11 wks old - ABX treated)
ABX treatment
SUP or Butyrate or Veh
-2
-1
0
1
2
3
days
SI
Tumor multiplicity (% relative to vehicle)
Veh
SUP
Butyrate
g
Lesion analysis
Axis lenght (µm)
Area (µm²)
****
***
*
****
Veh
SUP
Butyrate
h
AOM/DSS model (WT mice)
DSS 1.5%
AOM
SUP or Veh
8
9
10
11
12
13
14
weeks of age
Colon
ns
Tumor multiplicity (% relative to vehicle)
Veh
SUP
i
Lesion analysis
Axis length (µm)
Area (µm²)
**
*
Veh
SUP

Figure 5

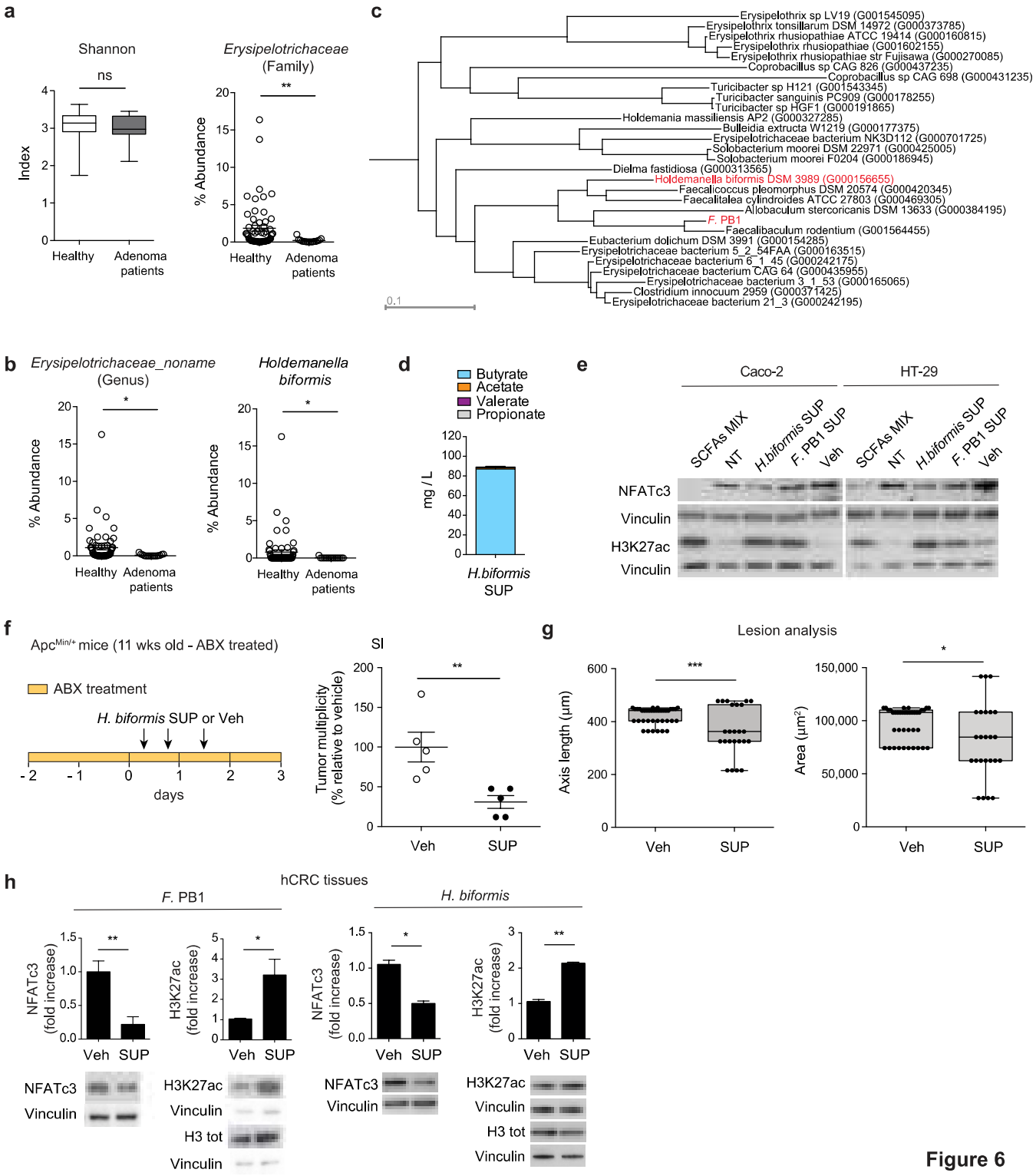
a
Shannon
ns
Index
Healthy
Adenoma patients
Erysipelotrichaceae (Family)
**
% Abundance
Healthy
Adenoma patients
c
Erysipelothrix sp LV19 (G001545095)
Erysipelothrix tonsillarum DSM 14972 (G000373785)
Erysipelothrix rhusiopathiae ATCC 19414 (G000160815)
Erysipelothrix rhusiopathiae (G001602155)
Erysipelothrix rhusiopathiae str Fujisawa (G000270085)
Coprobacillus sp CAG 826 (G000437235)
Coprobacillus sp CAG 698 (G000431235)
Turicibacter sp H121 (G001543345)
Turicibacter sanguinis PC909 (G000178255)
Turicibacter sp HGF1 (G000191865)
Holdemania massiliensis AP2 (G000327285)
Bulleidia extructa W1219 (G000177375)
Erysipelotrichaceae bacterium NK3D112 (G000701725)
Solobacterium moorei DSM 22971 (G000425005)
Solobacterium moorei F0204 (G000186945)
Dielma fastidiosa (G000313565)
Holdemanella biformis DSM 3989 (G000156655)
Faecalicoccus pleomorphus DSM 20574 (G000420345)
Faecalitalea cylindroides ATCC 27803 (G000469305)
Allobaculum stercoricanis DSM 13633 (G000384195)
F. PB1
Faecalibaculum rodentium (G001564455)
Eubacterium dolichum DSM 3991 (G000154285)
Erysipelotrichaceae bacterium 5_2_54FAA (G000163515)
Erysipelotrichaceae bacterium 6_1_45 (G000242175)
Erysipelotrichaceae bacterium CAG 64 (G000435955)
Erysipelotrichaceae bacterium 3_1_53 (G000165065)
Clostridium innocuum 2959 (G000371425)
Erysipelotrichaceae bacterium 21_3 (G000242195)
0.1
b
Erysipelotrichaceae_noname (Genus)
Holdemanella biformis
% Abundance
Healthy
Adenoma patients
d
Butyrate
Acetate
Valerate
Propionate
mg / L
H.biformis SUP
e
Caco-2
HT-29
SCFAs MIX
NT
H.biformis SUP
F. PB1 SUP
Veh
NFATc3
Vinculin
H3K27ac
Vinculin
f
Apc Min/+ mice (11 wks old - ABX treated)
ABX treatment
H. biformis SUP or Veh
days
SI
Tumor multiplicity (% relative to vehicle)
Veh
SUP
g
Lesion analysis
Axis length (µm)
Area (µm²)
Veh
SUP
h
hCRC tissues
F. PB1
H. biformis
NFATc3 (fold increase)
H3K27ac (fold increase)
Veh
SUP
NFATc3
Vinculin
H3K27ac
Vinculin
H3 tot
Vinculin

Figure 6